*GEOLOGICA CARPATHICA*, JUNE 2021, 72, 3, 195–212 https://doi.org/10.31577/GeolCarp.72.3.2

# U–Pb dating and composition of columbite from Vishteritsa: Implication for timing of granite magmatism and rare-element granitic pegmatites in the Western Rhodopes, Bulgaria

IRENA PEYTCHEVA[1,2,✉], ALBRECHT VON QUADT[2], VLADISLAV KOSTOV-KYTIN[3], MILEN KADIYSKI[4] and MILEN STAVREV[1]

[1]Geological Institute, Bulgarian Academy of Sciences, Acad. G. Bonchev str., bl. 24, 1113 Sofia, Bulgaria; ✉ipeytcheva@geology.bas.bg, milen_stavrev07@abv.bg
[2]Institute of Geochemistry and Petrology, ETH Zurich, 8092 Zurich, Switzerland; vonquadt@erdw.ethz.ch
[3]Institute of Mineralogy and Crystallography, Bulgarian Academy of Sciences, Acad. G. Bonchev Str., bl. 107, 1113 Sofia, Bulgaria; vkytin@abv.bg
[4]Aurubis Bulgaria AD, Research and Development, Industrial zone Pirdop, Bulgaria; m.kadiyski@aurubis.com

*(Manuscript received November 25, 2020; accepted in revised form June 16, 2021; Associate Editor: Milan Kohút)*

**Abstract:** The economic significance of pegmatites as a source of strategic rare metals for high-tech products and green energy motivated the present study on Ta–Nb oxides from Vishteritsa rare-element beryl–columbite LCT pegmatites of the Rila–West Rhodopes Batholith in the Western Rhodopes, Bulgaria. Here, we present the first U/Pb age data from columbite with application of the LA–ICP–MS U–Pb technique and a new X36 columbite standard reference material. The obtained Concordia age of 47.57±0.32 Ma with a small spread of the individual $^{206}Pb/^{238}U$ ages between 45 and 51.3 Ma argues for Early Eocene magmatism and pegmatite formation. The host granite of the rare-element pegmatites is dated 51.94±0.61 Ma with LA–ICP–MS U–Pb technique on zircon and suggests a fertile Early Eocene magmatic period in the Western Rhodopes. EPMA data for the composition of the columbite is used to refine the formula of the mineral $(Mn_{0.554}Fe_{0.427}U_{0.006})_{0.987}(Nb_{1.826}Ta_{0.085}Ti_{0.116})_{2.03}O_6$ and define it as columbite-(Mn). Application of the in-situ LA–ICP–MS data technique establishes a series of typical trace elements (Ti, U, Zr, Hf, Y, W, and Zn) that are usually found in content above 500 ppm. The studied columbite is enriched in heavy rare earth elements (HREE sum: 306–697 ppm) and depleted in light REE and Eu. These geochemical characteristics are collectively interpreted as evidence for crystallization from highly fractionated fluid-rich magma. High $UO_2$ content reaching 0.89 wt. % is characteristic for the Vishteritsa columbite. The decrease of U proximal to cracks and in outer crystal zones documents U-mobility during overprinting hydrothermal processes.

**Keywords:** columbite, pegmatite, Rhodopes, LA–ICP–MS U–Pb dating, X36 columbite SRM, trace elements.

## Introduction

Pegmatites have kept the interest of mineralogists, petrologists and economic geologists for hundreds of years due to their mineral diversity and generation complexity (e.g., Černý 1982; Galliski & Černý 2006; London 2008). A variety of geological processes on Bulgarian territory produced abundant granitic pegmatites of diverse morphology, structure, and mineralogical–geochemical features (Ivanov 1991). They were studied intensively in the 1960's and exploited for industrial minerals, mainly feldspars and micas, rarely quartz. The current revival of interest is related to the economic significance of pegmatites that are sources of strategic rare metals for high-tech products with application in electronics, aerospace, and green-energy production. This is stimulating the study of pegmatites and their constituent minerals worldwide. Here, we focus on the Vishteritsa granitic pegmatites in Western Rhodopes, Bulgaria (Figs. 1, 2), and one of their strategic minerals: columbite.

Columbite-group minerals are complex oxides with the general formula $AB_2O_6$, which have two structurally non-equivalent octahedral positions that can be occupied by the following cations: *A*-site: $Fe^{2+}$, $Fe^{3+}$, $Mn^{2+}$, $Mg^{2+}$, small to trace quantities of $Zn^{2+}$, $Ca^{2+}$, $Pb^{2+}$, $Sc^{3+}$, $Y^{3+}$, $Sb^{3+}$, $Zr^{4+}$, $Hf^{4+}$, $U^{4+}$, and $Th^{4+}$; *B*-site: $Nb^{5+}$, $Ta^{5+}$, with less amounts of $Fe^{3+}$, $Ti^{4+}$, $Sn^{4+}$, and $W^{6+}$ (e.g., Černý & Ercit 1989; Ercit 1994; Romer et al. 1996; Černý et al. 2007; Melcher et al. 2015; Lupulescu et al. 2018; Chládek et al. 2020). However, natural members of the columbite group show a degree of structural disorder where the above-mentioned cations are mixed between both *A* and *B* sites (e.g., Černý & Ercit 1989). The group includes Nb-dominant members: columbite-(Fe), columbite-(Mn) and columbite-(Mg), whereas Ta-dominant are tantalite-(Fe), tantalite-(Mn) and tantalite-(Mg).

Uranium concentration is sufficiently high in columbite-group minerals and they commonly contain almost no common lead, which make them suitable for U/Pb dating. Columbite U–Pb geochronology has been successfully applied to age

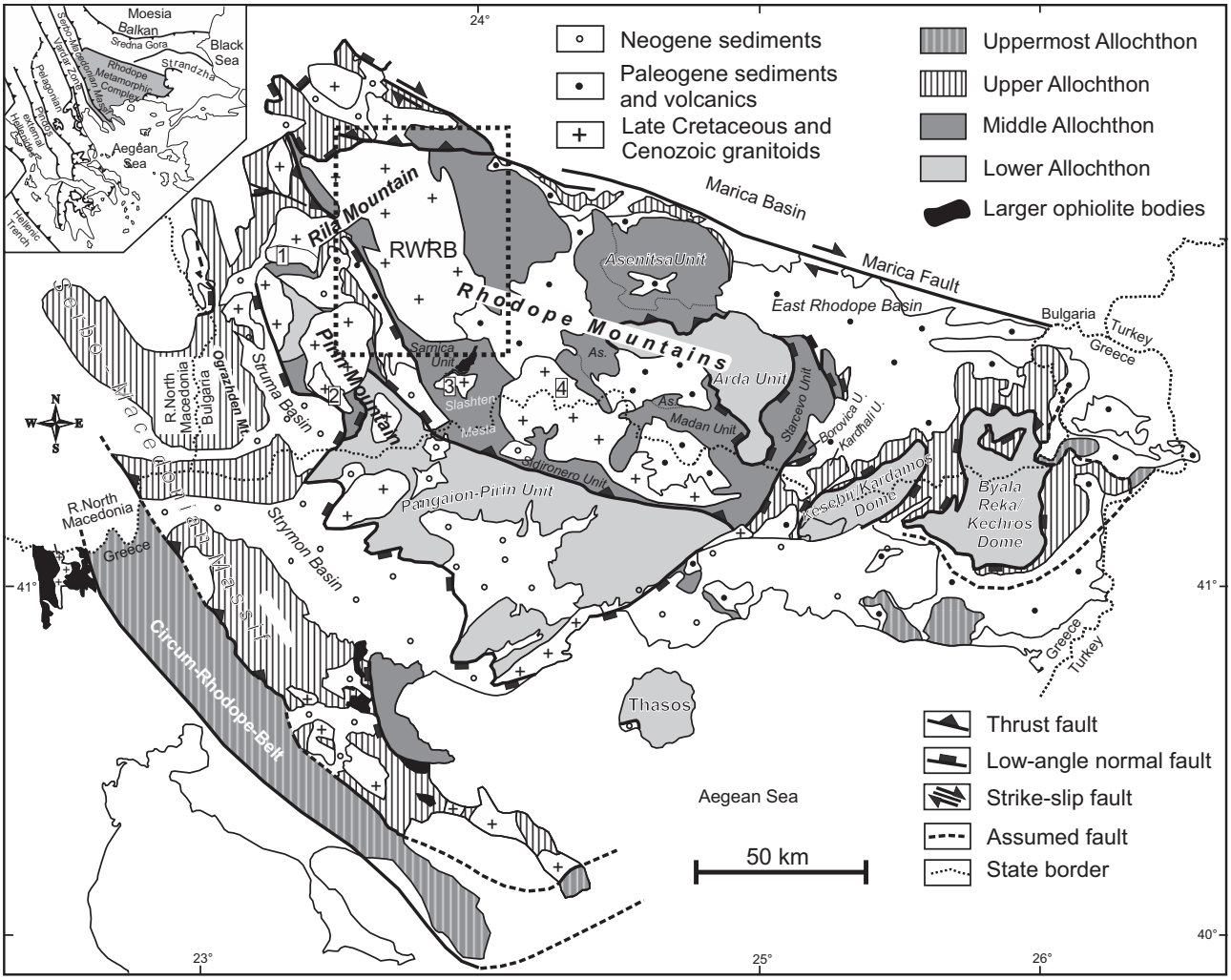


**Fig. 1.** Tectonic overview of the Rhodope Metamorphic Complex and its surroundings (modified after Burg et al. 1996; Ricou et al. 1998; Bonev et al. 2006; Sarov et al. 2008; Gorinova et al. 2019). Inset (upper left): tectonic sketch map of the Balkan Peninsula. Rectangle: outline of Fig. 2. Numbers 1–4: Early-Middle Eocene granitoids; 1 — Kapatnik granite; 2 — Spanchevo granite; 3 — Dolno Dryanovo granite; 4 — Barutin–Buynovo–Elatia granitoids; RWRB — Rila–West Rhodopes Batholith.

determination of granitic pegmatites (e.g., Romer & Wright 1992; Romer & Lehmann 1995; Romer et al. 1996; Romer & Smeds 1997; Baumgartner et al. 2006; Smith et al. 2004; Melleton et al. 2012; Deng et al. 2013; Che et al. 2015; Melcher et al. 2015; Lupulescu et al. 2018; Yan et al. 2018; Zhou et al. 2018). However, columbite-bearing ores are still difficult to date by conventional LA–ICP–MS U–Pb technique, as there is no matrix-matched standard reference materials (SRM) known. Several publications presented LA–ICP–MS ages of columbite, using zircon as the primary SRM (Che et al. 2015, 2019) but von Quadt et al. (2019) and Galliski et al. (2021) provided evidence for non-matrix-matched behaviour between zircon and columbite.

In this study, we present new data on columbite from Vishteritsa rare-element pegmatites in Bulgaria. They are hosted by the Rila–West Rhodopes batholith, a composite pluton of mainly granitic composition and Late Cretaceous to Palaeogene age. The LA–ICP–MS U–Pb technique and a new X36 columbite SRM (von Quadt et al. 2019) are used for age dating with the aim of establishing the time period of fertile granitic magmatism in the Western Rhodopes. Electron probe microanalyses and LA–ICP–MS techniques are applied to define the mineral composition and trace element variations of the biggest columbite crystal found in Vishteritsa and to understand the processes of rare-element pegmatite formation. The columbite age results are compiled with U–Pb LA–ICP–MS zircon data for the host granite to better constrain the fertile magmatism in the Western Rhodopes.

## Geological setting of Vishteritsa pegmatites

### *Regional geology*

The Rhodopes are the main tectonic unit on the Balkan Peninsula and referred to as the Rhodope Zone, or Rhodope

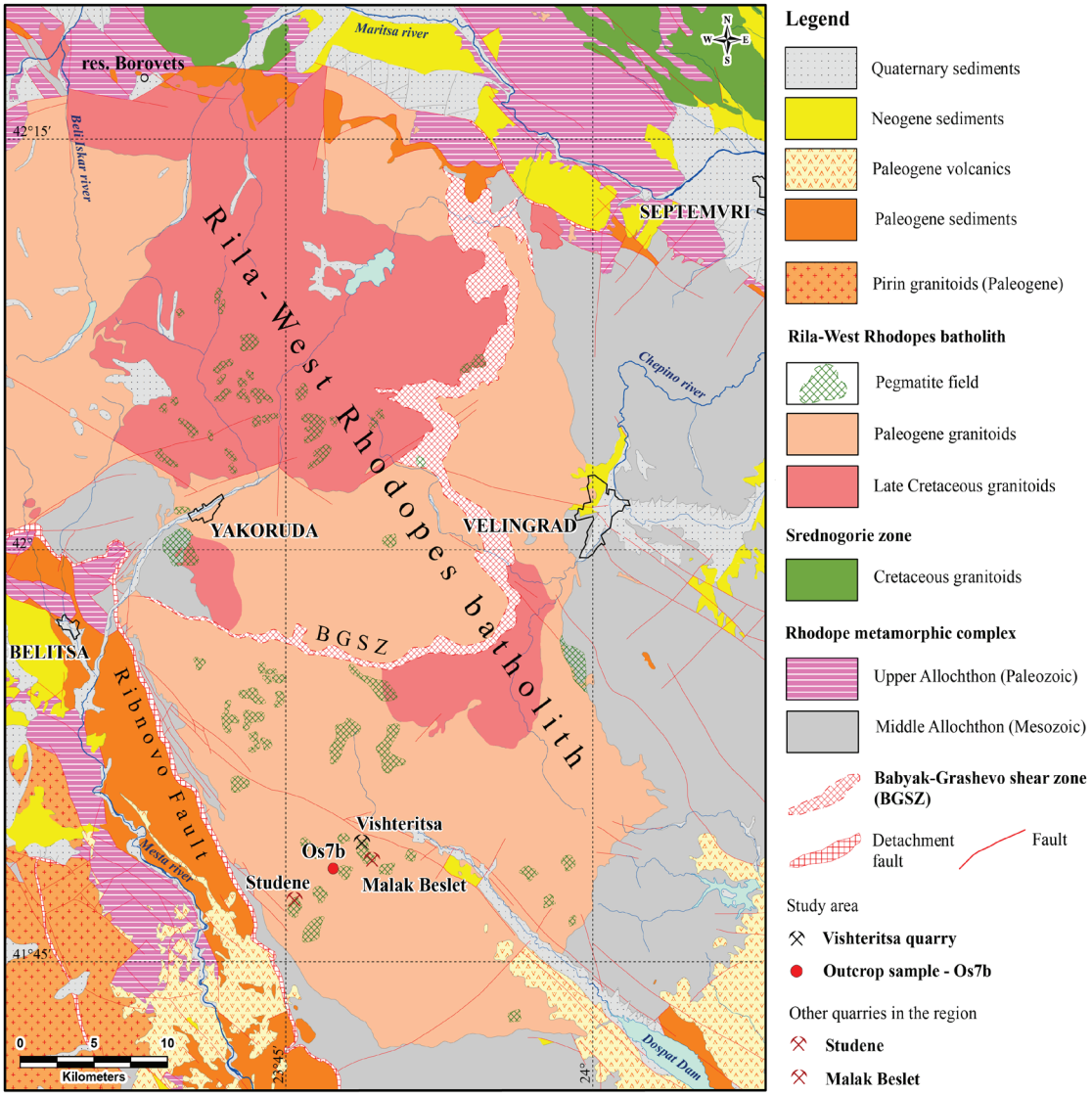


**Fig. 2.** Simplified geological map of the Rila–West Rhodope Batholith (modified after Valkov et al. 1989, Kamenov et al. 1999 and Stavrev et al. 2020) with the location of the rare-element pegmatite fields of the Vishteritsa, Studene and Malak Beslet, and Os7b granite sample.

Metamorphic Complex (RMC; Fig. 1). Tectonic interpretations agree on its complex Alpine (Late Jurassic to Late Oligocene) tectono–metamorphic history comprising earlier compressional and later extensional periods (e.g., Dinter & Royden 1993; Burg 2012; Froitzheim et al. 2014; Ivanov 2017; Schmid et al. 2020). The compressional tectonics resulted in the formation of a nappe stack. The RMC was primarily subdivided in three major units termed Lower, Intermediate, and Upper Terrane, according to their structural position (Burg et al. 1990, 1996). The Lower and the Upper Terranes represent continental fragments separated by several imbricated units (Intermediate Terrane), with ophiolitic and magmatic arc protoliths, thus interpreted as a suture zone (Burg 2012). The protolithic age of the Lower and Upper crustal terranes is Paleozoic to rarely Neoproterozoic with evidence for the Variscan metagranites that are exposed now in the cores of the Central Rhodopean (Arda) and Byala-Reka-Kechros Metamorphic Core Complexes (Peytcheva & Von Quadt 1995; Liati & Gebauer 1999; Ovtcharova et al. 2004; Kaiser-Rohrmeier et al. 2013; Naydenov et al. 2013; Liati et al. 2016). These units rarely preserve relics of Variscan UHP metamorphism (Janák et al. 2011), or Late Cretaceous HP metamorphism (Miladinova et al. 2018). Substantial data were also added for the Mesozoic Jurassic–Early Cretaceous and rarely Triassic protolithic age of the metamorphic rocks of the Intermediate terrane. (Sarov et al. 2008; Jahn-Awe et al. 2010; Turpaud & Reischman 2010). The latter bear evidence of HP and UHP metamorphism related to repeated subduction in the Late Jurassic–Early Cretaceous (Liati 2005; Turpaud & Reischman 2010; Liati et al. 2016), in the Late Cretaceous (Collings et al. 2016), and in the Late Palaeocene–Early Eocene time (Liati et al. 2016).

In the present study, we follow the regional-scale tectonic schemes proposed by Georgiev et al. (2010), Jahn-Awe et al. (2012) and Froitzheim et al. (2014). In their interpretation, the RMC is composed of four large, orogen-scale allochthonous thrust sheets, namely: Lower, Middle, Upper, and Uppermost Allochthons (Fig. 1). The first three tectonic units (thrust sheets) coincide generally with the Lower, Intermediate and Upper Terrane of Burg (2012), and the Uppermost Allochthon represents remnants of oceanic lithosphere referred as the Circum-Rhodope Triassic–Jurassic Tectonic Zone (Bonev & Stampfli 2008). An important difference between the two schemes is time and duration of the collision. In the former model it was accepted as Jurassic–Cretaceous while the south verging thrusting finished in Late Cretaceous–Earliest Paleocene time (Burg 2012); after a period of thermal relaxation, in the Middle Eocene and later, extensional tectonics affected the RMC triggered by mantle delamination (Burg 2012). In the latter, the Alpine orogeny was polycyclic and involved distinct episodes of subduction and crustal accretion (Gautier et al. 2017); the Late Alpine thrusting finished only in Mid-to-Late Eocene time and was still active in the lower parts of the nappe system, when the higher parts of the nappe pile were tectonically denudated (Georgiev et al. 2010; Jahn-Awe et al. 2010, 2012; Gorinova et al. 2019).

The extensional Early–Middle Eocene to Oligocene period in the RMC is characterized by extensive intrusive and extrusive magmatism (Harkovska et al. 1989; Marchev et al. 2013). The Early–Middle Eocene (56–40 Ma) granitoids (fig. 1 in Marchev et al. 2013) reveal adakite-like signatures resulting from high-pressure amphibole fractionation accompanied by trace-element rich accessory minerals and water suppressed plagioclase fractionation. Mantle underplating and interaction with the mid- to lower part of collision- and underplating-induced thickened crust in the Rhodopes are suggested to explain the favourable conditions for their formation (Marchev et al. 2013). This period is also defined as the time of the emplacement (thrusting) of the Middle Allochthon onto the Lower Allochthon of the RMC (Bosse et al. 2009; Jahn-Awe et al. 2012; Froitzheim et al. 2014). During the Late Alpine extensional stages (Late Eocene–Oligocene and Mid-Miocene), the thickened crust formed by the four allochthons, has been reshaped by low-angle detachment faults, formation of core-complexes, exhumation of migmatitic cores and granites together with parts of its high-grade periphery (Jahn-Awe et al. 2012; Kaiser-Rohrmeier et al. 2013; Froitzheim et al. 2014; Ivanov 2017). The Late Eocene to Oligocene extensional plutonic and volcanic rocks made the transition to normal calc-alkaline magmatism in the RMC (e.g., Harkovska et al. 1989; Marchev et al. 2005). Crustal extension also resulted in the formation of grabens filled mainly with Eocene-to-Quaternary marine-to-continental deposits (Fig. 1; e.g., Ivanov 2017).

One of the biggest plutons exposed in the western parts of the RMC is the Rila–West Rhodopes Batholith (RWRB; Figs. 1, 2). It is a composite pluton comprising granitoids of different ages (Valkov et al. 1989; Kamenov et al. 1999; Stavrev et al. 2020). Earlier Rb–Sr mineral and whole rock studies (Peytcheva et al., 1998) and subsequent U–Pb zircon and monazite dating (Kamenov et al. 1999; Peytcheva et al. 2007; Stavrev et al. 2020) argues for two major magmatic stages of the RWRB: Late Cretaceous (71–68 Ma) represented by hornblende–biotite and biotite granodiorites, and Paleogene (40 Ma) with biotite- and two-mica, leucocratic and aplitic granites. In the western embayment of the RWRB, a slightly foliated Kapatnik body of medium- to coarse-grained granites with up to 2–3 cm K-feldspar megacrysts is distinguished with its most probable age around 56–58 Ma (mean $^{206}Pb/^{238}U$ age of 60.7±1.7 Ma; Milovanov et al. 2010; Gerdjikov 2012), and small fine-grained aplitoid granites and pegmatites in the north-western part of Rila Mt. were dated at 48–52 Ma (Gorinova et al. 2019). The Late Cretaceous granitoids are suggested to be formed in a subduction setting (Kamenov et al. 1999; Gallhofer et al. 2015). The Paleogene granites are described as syn- to post-collisional, fractionated, crustal dominated, and $H_2O$-rich (Kamenov et al. 1999).

Extensive pegmatite dykes and fields are spatially related to the granitoids of the RWRB. They are hosted in the pluton or intrude the metamorphic basement. In the eastern, western and southern parts of the batholith the latter corresponds to the Middle Allochthone of the RMC (Georgiev et al. 2010; Froitzheim et al. 2014) and include a variety of metamorphic lithotectonic units: the Sarnitsa, Mesta, Slashten and Malyovitsa (Sarov et al. 2008; Georgiev et al. 2010). The metagranites, marbles, schists and amphibolites of the Jurassic Sarnitsa lithotectonic unit outcrop in the south-western part of the batholith and the region of the Vishteritsa pegmatites (Sarov et al. 2008).

### *Vishteritsa pegmatites*

Vishteritsa is a pegmatite field located about 40 km southwest of Velingrad town (Fig. 2) in the upper reaches of the Vishteritsa River. The pegmatite dykes (Fig. 3b) are hosted by coarse-grained and porphyritic biotite and two-mica granites (Fig. 3a) of Paleogene age. Close to Malak Beslet summit, the pegmatites were exploited for K-feldspar and muscovite until 1961. The biggest outcropped pegmatite body of the Vishteritsa deposit was a 13–15 m thick dyke striking NE 63° and dipping 36° with clear zonation (Arnaudov & Petrusenko 1967; Ivanov 1967, 1991). The geological cross-section through the pegmatite body, as it was described by Ivanov (1967), is shown on Fig. 3c. The latter distinguished 11 zones (Fig. 3c; see also Ivanov 1991, fig. 20) in the asymmetrically zonal pegmatite, formed subsequently from the contacts toward the central part of the vein. The first two outer "contact" zones were formed with a sharp contact to the hosting granite and are of quartz–oligoclase–microcline composition in the hanging part (Fig. 3c), or quartz–microcline composition in the laying part of the pegmatite. They are followed by a graphic quartz microcline zone on both sides. The next blocky quartz–microcline and quartz–microcline–clevelandite zones are better developed in the hanging part (Fig. 3c), in relation to both the size of

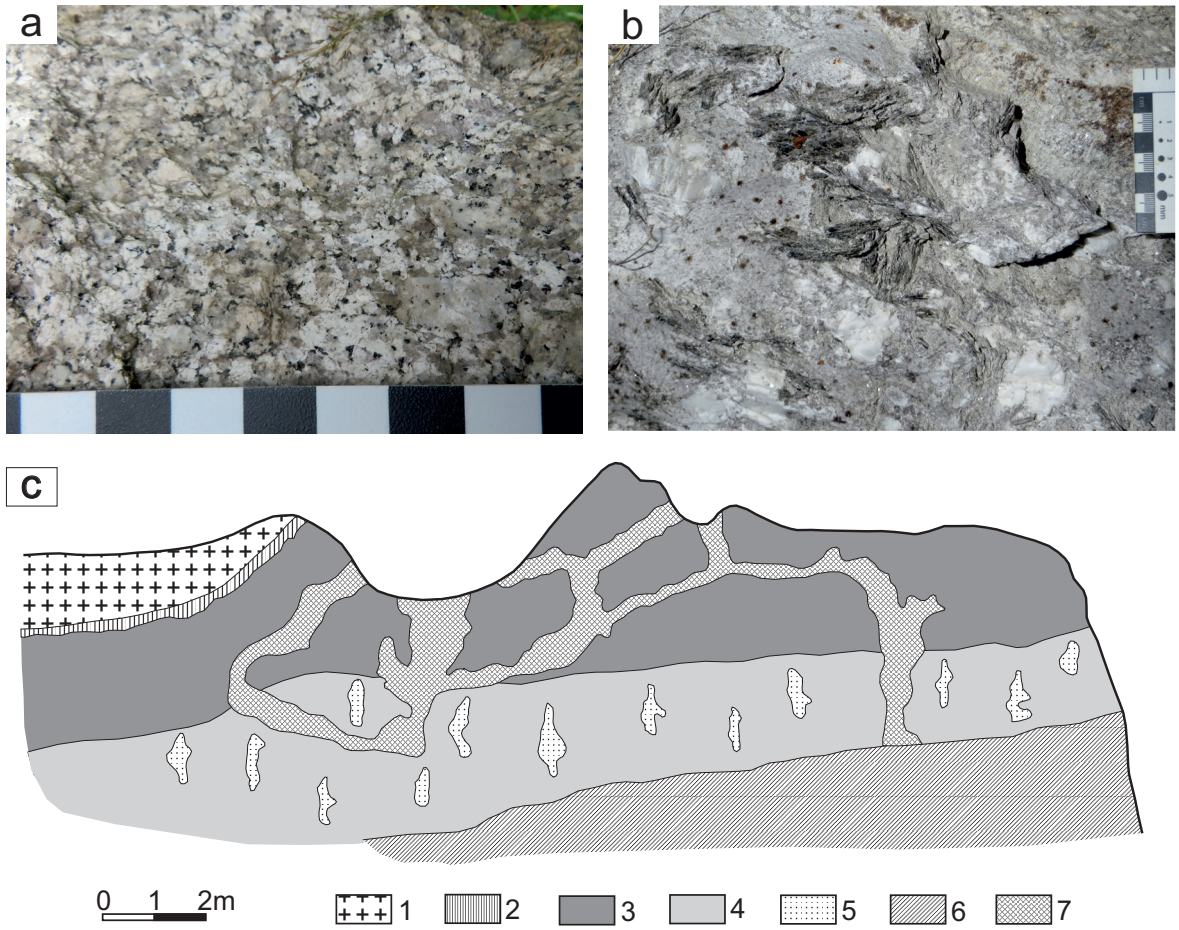


**Fig. 3.** Macrophotographs and a scheme of Vishterista pagmatites and the RWRB granite in the study area. **a** — Macrophotograph of the coarse grained biotite granite Os7b hosting the Vishteritsa pegmatites; **b** — Quartz–muscovite–albite zone with garnet from a smaller pegmatite of the Vishteritsa pegmatite field; **c** — Cross-section of part of the big Vishteritsa pegmatite (after Ivanov 1967, 1991). Legend: 1 — granite; 2 — quartz-oligiclase-microcline contact zone; 3 — graphic quartz-microcline zone; . 4 — blocky quartz–microcline zone with nests (5) filled by smoky quartz, albite, muscovite, gahnite, monazite, xenotime and columbite; 6 — quartz–muscovite–clevelandite zone; 7 — quartz–muscovite–albite alteration complex replacing parts of the graphic and blocky quartz–microcline zones.

the zones (>2 m each) and of the crystals (1.0–1.5 m single microcline crystal), and are followed by a zone of blocky quartz with some nests of microcline or coarse crystalline muscovite. In the laying part, from the graphic towards the blocky quartz zone a series of albite dominated zones were formed – apographic quartz–albite zone, aplitoid banded quartz–albite and quartz–garnet–albite zone, medium-grained albite zone (2 m thick), and finally a quartz–muscovite–clevelandite zone (only 15–20 cm thick). Mainly in the hanging part of the pegmatite, veinlets and nests of quartz–muscovite–albite are formed and considered as alteration and replacement in the graphic and blocky quartz–microcline zones (Fig. 3c; Ivanov 1967, 1991).

The main constituent minerals of the Vishteritsa pegmatite are K-feldspar (microcline), quartz, albite and muscovite, rarely oligoclase and biotite. Accessory minerals include magnetite, ilmenite, amphibole, apatite, zircon, monazite, xenotime, columbite, garnet, beryl, and gahnite (Arnaudov & Petrusenko 1967; Ivanov 1967). A well-expressed trend of increase of the Mn, Hf, U, REE and Ta content towards the internal zones of the pegmatite is described (Arnaudov & Petrusenko 1967). The size and amount of rare-element minerals increase in the same direction (Arnaudov & Petrusenko 1967). The columbite is found in all pegmatite zones except the contact and graphic zones, and the blocky quartz zone of the hanging part. The maximum amount of columbite was described in the banded quartz–albite zone (2183 ppm; Ivanov 1991). In the rest of the albite-dominated zones of the pegmatite, including the "replacement" quartz–albite–muscovite zones, the columbite content was significantly lower (18–30 and 2 ppm, respectively; Ivanov 1991).

The pegmatite is classified as albite–microcline type by Ivanov (1991). According to its mineral association and the considered generic relation to the crustal-dominated Paleogene granites it can be assigned as LCT (lithium–caesium–tantalum) family rare-element class beryl–columbite subtype pegmatite (Černý & Ercit 2005; Černý et al. 2012).

The biggest Vishteritsa pegmatite was dated by Arnaudov et al. (1969) using U–Pb isotope method and the Isotope Dilution–Thermal Ionization Mass-Spectrometry (ID–TIMS) techniques

on zircon (cyrtolite variety, a hydrous Hf, U, Th, and REE-rich zircon). The obtained $^{206}Pb/^{238}U$ and $^{207}Pb/^{235}U$ ages 50±5 and 50±10 Ma overlap in their uncertainties. Boyadzhiev & Lilov (1976) reported K–Ar age around 50 Ma for a muscovite from the pegmatite.

## Previous investigations on columbite from the Vishteritsa pegmatite

The Vishteritsa pegmatite deposit is the second locality in Bulgaria where columbite was found and described (Breskovska 1962). In the quartz–muscovite–cleavelandite (platy albite) zone of the big Vishteritsa pegmatite, Breskovska (1962) described columbite crystals with size of up to 10 cm (exceptionally 20 cm). Ten crystal forms have been identified by Breskovska (1962): four bipyramids, four prisms, and two pinacoids. The habitus of the columbite crystals in all zones is similar but in the outer zones they are not well shaped, whereas in the core zone, more forms are observed and the two pinacoids {100} and {010} dominate (Arnaudov & Petrusenko 1967).

In order to obtain data on the chemical composition of columbite from this locality, Yordanov et al. (1962) subjected to analysis a well-shaped crystalline piece weighting ~250 g. The authors have applied classical chemistry techniques for the analysis with some modifications. Based on the data obtained, Breskovska (1962) reported the following crystal chemical formula for the mineral: $(Fe_{0.52}Mn_{0.39}U_{0.02})_{0.93}(Nb_{1.77}Ta_{0.12}Ti_{0.15})_{2.04}O_6$. Using averaged results from X-ray spectral studies, Arnaudov & Petrusenko (1967) and Ivanov (1991) reported new data on the chemical composition of columbite that allow the following crystal chemical formula to be deduced: $(Fe_{0.71}Mn_{0.40}U_{0.03})_{1.14}(Nb_{1.69}Ta_{0.17}Ti_{0.09})_{1.95}O_6$.

Even at that time, researchers noticed contamination of the mineral with rutile, uraninite and other secondary uranium minerals, which very finely penetrate cracks and replace columbite (Breskovska 1962; Yordanov et al. 1962). This makes the results of the former old analytical techniques for the definition of chemical composition very dependent on the presence of impurities. Yordanov et al. (1962) concluded that the secondary uranium minerals closely associate with the columbite and influence its geological age.

Recently, Kostov-Kytin et al. (2020) provided new Scanning Electron Microscopy (SEM), Energy-Dispersive X-ray Spectroscopy/Analysis (EDS/EDXA), and single crystal X-ray Diffraction Analysis (SXDA) studies on columbite from Vishteritsa. Based on the single crystal studies in that work and the chemical analyses performed by previous researchers on Vishteritsa columbite samples, the mineral was defined as columbite-(Fe). Its crystal chemical formula derived by SXDA is as follows: $(Nb_{0.54}Mn_{0.30}Pb_{0.016})(Nb_{0.69}Fe_{0.16}Ti_{0.055}Ta_{0.035})_2O_6$. The content of U is quite low to allow unambiguous detection of its positions in the structure. Backscattered electron (BSE) studies show the presence of zoning induced by variations in the chemical composition of the sample used for single crystal studies. Uranium is completely missing in one of the zones ("high-grey-level" zone) and its content reaches 0.04 apfu in the other "low-grey-level" one. However, this zonation does not disturb the diffraction pattern observed with SXDA which characterizes the studied sample as a single-phase one. With some caution, Kostov-Kytin et al. (2020) concluded that the columbite from Vishteritsa can be used for U–Pb dating. A prerequisite for this is the finding of a compositionally homogeneous site in the mineral to exclude the possibility of contamination with primary or secondary uranium mineralization.

## Materials and analytical techniques

Fragments of a crystalline columbite sample from the Vishteritsa pegmatite described previously by Breskovska (1962) and currently preserved in the National Museum of Natural History at the Bulgarian Academy of Sciences, Sofia, were used for the present studies (Figs. 4, 5).

### *Electron probe microanalyses (EPMA)*

Electron probe microanalyses were done on a polished, carbon-coated section of a columbite crystal using INCA Wave700 detector (WDS, Oxford Instruments) with six diffracting crystals, installed on a TESCAN VEGA 3 XMU scanning electron microscope (@20 kV accelerating voltage) at the Research and Development Department of Aurubis Bulgaria AD, Pirdop. The spectra were collected on O$K_\alpha$, Ti$K_\alpha$, Mn$K_\alpha$, and Fe$K_\alpha$, lines with standards of natural magnetite and pure $TiO_2$ and $MnO_2$ by Geller Microanalytical Laboratory Inc. EDS spectra were collected using X-Max$^N$ 50 EDS detector by Oxford Instruments with factory standards. AztecWave software was used for data collection, integration and corrections. Selected results from EPMA are listed in Table 1. SEM backscattered images are shown on Fig. 5.

**Fig. 4.** Columbite crystal from the Vishteritsa pegmatite, Western Rhodopes, Bulgaria. Macrophotography of studied sample from the National Museum of Natural History at the Bulgarian Academy of Sciences, Sofia. Sample size: 21×17×8 cm.

### *Cathode-luminescent (CL) zircon imaging*

The internal zircon patterns were documented by cathode-luminescent (CL) images using a JEOL JSM-6610 LV SEM-EDS at the University of Belgrade, Serbia.

### *Laser ablation inductively coupled plasma mass spectrometry (LA–ICP–MS)*

The LA–ICP–MS method was applied for in situ U–Pb dating of columbite. Analytical work was performed employing the equipment at the Geological Institute (BAS) – a NWR UP193 FX laser ablation system combined with PerkinElmer ELAN DRC-e ICP-mass spectrometer. The operating conditions, data acquisition parameters, measured isotopes, and standardization are summarized in Table 2. The results of U–Pb geochronology were calculated using Iolite data reduction program (Paton et al. 2011) combined with VisualAge to obtain ages and ratios corrected for instrumental drift and down-hole fractionation. The plots were processed using ISOPLOT 3.0 or ISOPLOT 4.15 (Ludwig 2003). Columbite U–Pb dating represents Concordia age shown on normal

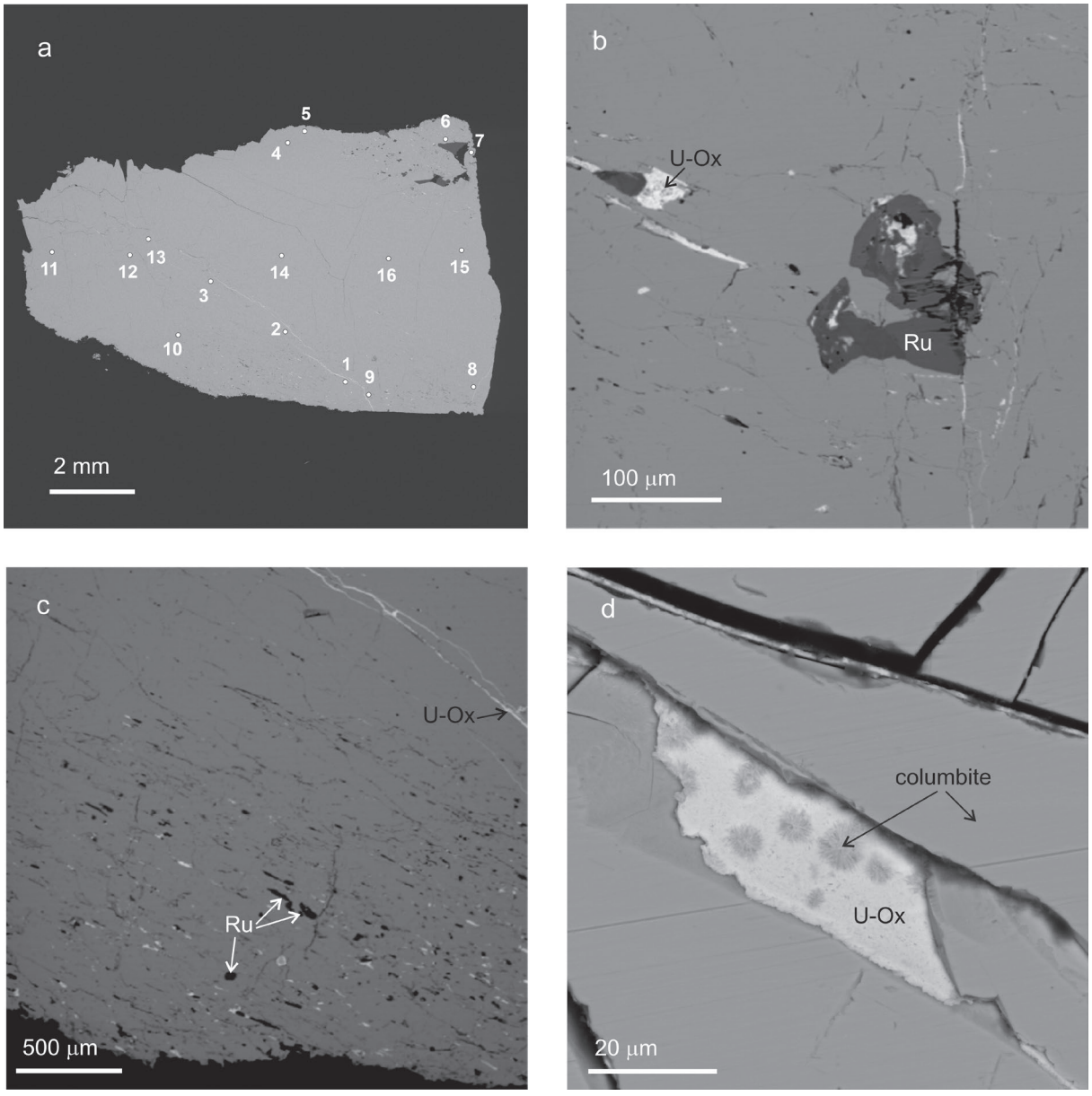


**Fig. 5.** Backscattered electron images of a fragment of the crystal shown on Fig. 4, used for U–Pb and geochemical studies. The circles on 5a show the position of laser-ablation craters for the major and trace element analyses, accompanied by contemporary U–Pb dating (*italic numbers 1–16* of Table 3). Position of the craters for dating only were randomly chosen but followed generally a profile from the outer to the central zones. The images on 5b, c and d show parts of the same crystal with uranium oxides (U-Ox) in cracks and pits (b, c and d) and small rutile (Ru) crystals in holes (c).

**Table 1:** Selected electron microprobe analyses of columbite from Vishteritsa pegmatite, Western Rhodopes.

| Element wt. % | 1 | 2 | 3 | 4 | 5 | 6 | 7 | 8 | 9 | 10 | 11 | 12 | 13 | average | mole units | atom units normalized to 6 atoms O | |
|---|---|---|---|---|---|---|---|---|---|---|---|---|---|---|---|---|---|
| Fe | 6.821 | 6.873 | 6.951 | 7.060 | 6.987 | 6.981 | 6.821 | 6.919 | 6.876 | 6.796 | 6.983 | 6.947 | 6.890 | 6.916 | 0.12383 | | 0.427 |
| Mn | 8.924 | 9.064 | 8.761 | 8.929 | 8.739 | 8.916 | 8.791 | 8.871 | 8.793 | 8.795 | 8.781 | 8.767 | 8.770 | 8.839 | 0.16088 | | 0.554 |
| U | 0.341 | 0.396 | 0.428 | 0.433 | 0.371 | 0.377 | 0.378 | 0.371 | 0.358 | 0.399 | 0.374 | 0.648 | 0.477 | 0.411 | 0.00173 | | 0.006 |
| | | | | | | | | | | | | | | | | A site total | 0.987 |
| Nb | 49.524 | 49.545 | 48.955 | 49.746 | 49.258 | 49.134 | 49.163 | 49.021 | 48.993 | 49.096 | 49.202 | 49.103 | 49.207 | 49.227 | 0.52983 | | 1.826 |
| Ta | 4.495 | 4.439 | 4.504 | 4.466 | 4.451 | 4.485 | 4.365 | 4.388 | 4.352 | 4.402 | 4.413 | 4.603 | 4.598 | 4.459 | 0.02464 | | 0.085 |
| Ti | 1.535 | 1.536 | 1.681 | 1.678 | 1.580 | 1.615 | 1.573 | 1.590 | 1.627 | 1.593 | 1.599 | 1.677 | 1.696 | 1.614 | 0.03371 | | 0.116 |
| W | 0.200 | 0.155 | 0.157 | 0.207 | 0.186 | 0.159 | 0.136 | 0.181 | 0.173 | 0.119 | 0.173 | 0.072 | 0.096 | 0.155 | 0.00084 | | 0.003 |
| | | | | | | | | | | | | | | | | B site total | 2.030 |
| O | 27.879 | 27.689 | 27.878 | 27.794 | 27.443 | 27.518 | 27.478 | 27.350 | 27.197 | 27.727 | 27.488 | 29.299 | 29.393 | 27.856 | 1.74102 | | 6 |
| | | | | | | | | | | | | | | | | | |
| | | | | | | | | | | | | | | | | Mn/(Mn+Fe) | 0.565 |
| Total | 99.72 | 99.70 | 99.32 | 100.31 | 99.02 | 99.19 | 98.71 | 98.70 | 98.37 | 98.93 | 99.01 | 101.11 | 101.13 | 99.48 | | Ta/(Ta+Nb) | 0.044 |

Crystal chemical formula of the Vishteritsa columbite based on 13 WDS analyses $(Mn_{0.554}Fe_{0.427}U_{0.006})_{0.987}(Nb_{1.826}Ta_{0.085}Ti_{0.116}W_{0.003})_{2.03}O_6$.

Concordia diagram. The X36 columbite (354.8±1.7 Ma; Galliski et al. 2021) was used as the primary external standard for dating, and NIST610 as primary external standard for trace elements. For the U–Pb isotope zircon analyses of the hosting granite a laser-crater of 35 μm diameter, repetition rate 8 and fluency of 7 were applied, using the GJ1 as primary and Plešovice zircon as secondary standard reference material (SRM). During the daily session, the Plešovice SRM was dated at 337.9±4 Ma. The chemical composition of the columbite was calculated assuming 100 % sum of the main oxides, then the niobium content was used as the internal standard to calculate the trace elements, applying SILLS data reduction program (Guillong et al. 2008).

## Results

### *LA–ICP–MS in situ U–Pb dating*

Sixteen in-situ LA–ICP–MS U–Pb analyses of columbite were performed on two different days with the same analytical conditions (data in normal font in Table 3). Additional fourteen U–Pb dating analyses were performed at the same time as trace-element measurements of columbite (Fig. 5; analyses 17–25 in Table 3, italic font). The obtained U/Pb results are presented in Table 3 and plotted on Fig 6. The individual analyses are mostly concordant and the $^{206}Pb/^{238}U$ ages spread from 51.6±2.5 Ma to 44.9±3.3 Ma. Excluding the two analyses with an apparent age older than 50 Ma and the youngest point with higher analytical uncertainty, a Concordia age of 47.57±0.32 Ma (95 % confidence, decay-constant errors included, MSWD of concordance=5.9) can be calculated.

The zircons of the host granite reveal oscillatory magmatic zonation, often with brighter cores and darker outer parts that are related to high uranium content (Table 4). Twenty-six analyses of the zircons mainly in the outer parts of the grains are dated and most of the U/Pb data are in the range of 49–53 Ma (Table 4, Fig. 7a–d). One tinny grain shows some lead loss (apparent age 46–47 Ma, Fig. 7a) and two reveal negligible inheritance (54–56 Ma). Two zircon grains with magmatic oscillatory zonation are older and show concordant ages at 143 and 71 Ma, respectively (Fig. 7c) and are interpreted as contamination from the host rocks (Late Cretaceous RWRB granites and Jurassic metagranites of the Surnitsa lithotectonic unit). Excluding the outliers, twenty zircon analyses define a Concordia age of 51.94±0.61 Ma (Fig. 7d).

### *Columbite composition and trace element geochemistry*

Thirteen EPMA analyses were performed on a small apparently unaltered fragment of the columbite crystal apart from cracks and visible inclusions and the results are shown in Table 1. The data are used to calculate an average formula $(Mn_{0.554}Fe_{0.427}U_{0.006})_{0.987}(Nb_{1.826}Ta_{0.085}Ti_{0.116}W_{0.003})_{2.03}O_6$. The major elements (Nb, Ta, Fe, Mn) content does not vary significantly

**Table 2:** LA–ICP–MS operating conditions for U–Pb geochronology and trace element composition (tracing) of columbite from Vishteritsa, Western Rhodopes, Bulgaria.

| **Equipment** | **Geological Institute, BAS** | |
|---|---|---|
| *ICP–MS* | PerkinElmer SCIEX ELAN DRC-e | |
| Forward power (W) | 1500 | |
| Gas flow rate (l·min$^{-1}$): | | |
| Nebulizer (Ar) | 0.80 | |
| Auxiliary (Ar) | 0.92 | |
| Plasma (Ar) | 15.0 | |
| Carrier (He) | 0.92 | |
| Lens voltage | 7 | |
| Oxide production rate | $ThO^+/Th^+$ <0.5 % | |
| Laser Ablation System | New Wave UP193FX | |
| Wavelenght (nm) | 193 | |
| Energy density on sample (J cm$^{-2}$) | 4.6–4.7 | |
| Repetition rate (Hz) | 2 | |
| Spot size (μm) | 20 | |
| Pulse duration (ns) | 4 | |
| *Data acquisition* | *Dating* | *Tracing* |
| Data acquisition protocol | Time resolved analysis | Time resolved analysis |
| Scanning mode | Peak hopping, 1 point per peak | Peak hopping, 1 point per peak |
| Sweeps | 1 | 1 |
| Reading/Replicate | 860 | 250 |
| Replicate | 1 | 1 |
| Background and signal acquisition | ~40 s gas blank and ~50–60 s ablation | ~40 s gas blank and ~50–60 s ablation |
| Dwell time per isotope: | 20 ms ($^{208}$Pb and $^{232}$Th); 30 ms ($^{206}$Pb, $^{207}$Pb, and $^{238}$U) | 20 ms ($^{208}$Pb and $^{232}$Th); 30 ms ($^{206}$Pb, $^{207}$Pb, and $^{238}$U); all others – 10 ms |
| Isotopes analyzed | $^{206}$Pb, $^{207}$Pb, $^{208}$Pb, $^{232}$Th, $^{238}$U | $^{27}$Al, $^{29}$Si, $^{31}$P, $^{42}$Ca, $^{45}$Sc, $^{49}$Ti, $^{51}$V, $^{55}$Mn, $^{57}$Fe, $^{59}$Co, $^{60}$Ni, $^{63}$Cu, $^{66}$Zn, $^{89}$Y, $^{91}$Zr, $^{93}$Nb, $^{97}$Mo, $^{107}$Ag, $^{118}$Sn, $^{139}$La, $^{140}$Ce, $^{141}$Pr, $^{146}$Nd, $^{147}$Sm, $^{151}$Eu, $^{157}$Gd, $^{159}$Tb, $^{163}$Dy, $^{165}$Ho, $^{167}$Er, $^{169}$Tm, $^{173}$Yb, $^{175}$Lu, $^{178}$Hf, $^{181}$Ta, $^{184}$W, $^{206}$Pb, $^{207}$Pb, $^{208}$Pb, $^{232}$Th, $^{238}$U |
| *Standardization* | | |
| External: | X36 columbite[a] | NIST610 |
| *Data reduction software*: | Iolite | Iolite, Sills |

[a] Data for external standard X36 is according to Galliski et al. (2021);
[b] Paton et al. 2011.

in the chosen crystal part and the mineral is defined as columbite-(Mn) (Fig. 8a).

The crystal fragment is studied with sixteen LA–ICP–MS analyses to better follow the compositional variations of major and trace elements of the columbite. The results show some small differences for the major elements (Nb, Ta, Mn, Fe, Ti) compared with EPMA analyses, however these are not significant (Table 5 and Fig. 8a) and the data can be used to outline spatial compositional trends. The $Nb_2O_5$ content is the highest and varies between 65.4 wt. % and 68.8 wt. %. The compositional variations of the major elements compiled with Zr and W (Table 5) are shown on Fig. 8b–f. They infer possible cationic substitutions with better correlations ($R^2$=0.87–0.95) of the elements in the unaltered crystal parts away from cracks and other defects (the grey squares of Fig. 8b–f corresponding to points 11–16 on Fig. 5a) compared to the analyses next to fractures and pits that are filled with secondary minerals (shown with crosses; points 1–9 on Fig. 5a).

The U content (1220–7823 ppm; 0.23–0.89 wt. % $UO_2$) doesn't show a regular distribution within the crystal but it rather depends on the proximity to cracks, porous and outer zones. There, U reveals the lower concentrations (Table 5 and Fig. 9a), opposite to cracks and pits themselves, which are filled with a uranium-oxide phase (Fig. 5b,c,d). Other trace elements of the columbite in higher concentration are Zr (2434–6755 ppm), Y (278–486 ppm), W (900–1860 ppm), Hf (130–580 ppm), and Zn (417–1097 ppm) (Table 5, Fig. 9a). Thorium content (9–96 ppm) is significantly lower than U, whereas Th/U ration varies from 0.004 to 0.021. Scandium and tin are other typical trace elements but their content stays below 100 ppm.

The rare-earth elements (REE) in the columbite of Vishteritsa are in the range 356–733 ppm (sum of REE, Table 5). The mineral is enriched in heavy REE (HREE: 306–697 ppm) and depleted in light REE (LREE), the latter often being below the limit of detection (LOD). Europium (Eu) has a very low concentration below LOD. For the chondrite-normalized plot of REE on Fig. 9b we used the LOD values of LREE (except for Sm). REE pattern reveal a clear trend of increase of the normalized values from LREE to HREE with a deep Eu anomaly and possible negative Ce anomaly (one exception for analysis 9). A negligible enrichment of HREE in the analyses close to cracks and outer zones of the columbite is revealed (grey lines on Fig. 9b; for the position of the points see Fig. 5a) compared with the unaltered zones (black lines on Fig. 9b) but there are also exceptions from the common trend.

**Table 3:** LA–ICP–MS U–Pb in-situ isotope data for columbite from Vishteritsa, Western Rhodopes, Bulgaria.

| N | Source file | $^{207}Pb/^{235}U$ | 2SE | $^{206}Pb/^{238}U$ | 2SE | Rho* | $^{207}Pb/^{206}Pb$ | 2SE | $^{207}Pb/^{235}U$ age, Ma | 2SE | $^{206}Pb/^{238}U$ age, Ma | 2SE |
|---|---|---|---|---|---|---|---|---|---|---|---|---|
| 1 | 20fe23g04 | 0.045 | 0.007 | 0.0072 | 0.0002 | 0.006 | 0.044 | 0.007 | 42 | 7 | 46.2 | 1.4 |
| 2 | 20fe23g05 | 0.046 | 0.009 | 0.0073 | 0.0003 | 0.020 | 0.042 | 0.009 | 44 | 9 | 46.8 | 1.6 |
| 3 | 20fe23g06 | 0.050 | 0.005 | 0.0075 | 0.0002 | 0.018 | 0.046 | 0.005 | 49 | 5 | 47.9 | 1.0 |
| 4 | 20fe23g07 | 0.047 | 0.006 | 0.0074 | 0.0002 | 0.040 | 0.042 | 0.005 | 46 | 5 | 47.6 | 1.1 |
| 5 | 20fe23g08 | 0.050 | 0.004 | 0.0075 | 0.0001 | 0.032 | 0.046 | 0.004 | 49 | 4 | 48.2 | 0.9 |
| 6 | 20fe23g09 | 0.048 | 0.004 | 0.0073 | 0.0002 | 0.116 | 0.050 | 0.005 | 47 | 4 | 47.0 | 1.4 |
| 7 | 20fe23g10 | 0.045 | 0.007 | 0.0071 | 0.0002 | 0.060 | 0.045 | 0.008 | 45 | 7 | 45.8 | 1.6 |
| 8 | 20fe23g11 | 0.052 | 0.015 | 0.0075 | 0.0004 | 0.035 | 0.076 | 0.025 | 44 | 14 | 47.8 | 2.5 |
| 9 | 20fe23g12 | 0.055 | 0.012 | 0.0080 | 0.0004 | 0.018 | 0.065 | 0.015 | 51 | 12 | 51.6 | 2.5 |
| 10 | 20fe23g13 | 0.046 | 0.010 | 0.0074 | 0.0003 | 0.058 | 0.045 | 0.010 | 43 | 9 | 47.5 | 1.8 |
| 11 | 20ja23f04 | 0.047 | 0.004 | 0.0074 | 0.0001 | 0.031 | 0.045 | 0.004 | 46 | 3 | 47.6 | 0.8 |
| 12 | 20ja23f05 | 0.051 | 0.004 | 0.0073 | 0.0001 | 0.089 | 0.049 | 0.004 | 50 | 4 | 46.8 | 0.8 |
| 13 | 20ja23f06 | 0.048 | 0.003 | 0.0073 | 0.0001 | 0.013 | 0.046 | 0.003 | 47 | 3 | 47.1 | 0.7 |
| 14 | 20ja23f07 | 0.053 | 0.007 | 0.0072 | 0.0002 | 0.006 | 0.052 | 0.007 | 51 | 6 | 46.3 | 1.2 |
| 15 | 20ja23f08 | 0.054 | 0.004 | 0.0075 | 0.0001 | 0.075 | 0.051 | 0.004 | 53 | 4 | 48.4 | 0.9 |
| 16 | 20ja23f09 | 0.050 | 0.004 | 0.0076 | 0.0001 | 0.005 | 0.047 | 0.003 | 49 | 3 | 49.0 | 0.8 |
| *1* | *21fe10b07* | *0.042* | *0.021* | *0.0070* | *0.0005* | *0.117* | *0.042* | *0.022* | *38* | *20* | *44.9* | *3.3* |
| *2* | *21fe10b08* | *0.056* | *0.009* | *0.0077* | *0.0003* | *0.051* | *0.053* | *0.009* | *54* | *9* | *49.5* | *1.8* |
| *3* | *21fe10b09* | *0.044* | *0.009* | *0.0075* | *0.0004* | *0.095* | *0.045* | *0.010* | *45* | *9* | *48.2* | *2.3* |
| *4* | *21fe10b10* | *0.057* | *0.011* | *0.0077* | *0.0004* | *0.011* | *0.053* | *0.010* | *57* | *11* | *49.3* | *2.5* |
| *5* | *21fe10b11* | *0.061* | *0.013* | *0.0079* | *0.0004* | *0.100* | *0.054* | *0.011* | *59* | *12* | *50.8* | *2.3* |
| *6* | *21fe10b12* | *0.043* | *0.009* | *0.0071* | *0.0004* | *0.014* | *0.046* | *0.010* | *43* | *9* | *45.4* | *2.3* |
| *7* | *21fe10b13* | *0.050* | *0.012* | *0.0070* | *0.0004* | *0.110* | *0.051* | *0.012* | *49* | *12* | *45.0* | *2.2* |
| *10* | *21fe10b18* | *0.049* | *0.010* | *0.0075* | *0.0004* | *0.090* | *0.048* | *0.010* | *48* | *10* | *47.9* | *2.3* |
| *11* | *21fe11c06* | *0.054* | *0.013* | *0.0074* | *0.0006* | *0.055* | *0.058* | *0.015* | *52* | *13* | *47.3* | *3.8* |
| *12* | *21fe11c07* | *0.049* | *0.014* | *0.0073* | *0.0005* | *0.294* | *0.047* | *0.013* | *47* | *13* | *46.5* | *3.4* |
| *13* | *21fe11c08* | *0.052* | *0.012* | *0.0073* | *0.0004* | *0.298* | *0.052* | *0.012* | *51* | *11* | *46.6* | *2.8* |
| *14* | *21fe11c09* | *0.051* | *0.013* | *0.0072* | *0.0004* | *0.064* | *0.050* | *0.013* | *49* | *12* | *46.4* | *2.7* |
| *15* | *21fe11c10* | *0.056* | *0.012* | *0.0074* | *0.0004* | *0.095* | *0.057* | *0.012* | *55* | *11* | *47.2* | *2.7* |
| *16* | *21fe11c11* | *0.051* | *0.012* | *0.0073* | *0.0004* | *0.018* | *0.055* | *0.013* | *49* | *11* | *46.6* | *2.4* |

* Rho=error correlation of $^{206}Pb/^{238}U$–$^{207}Pb/^{235}U$;

*Remark:* normal font (1–16) is used for dating LA–ICP–MS analyses, italic – for contemporary dating and tracing LA–ICP–MS analyses (analytical conditions in Table 2);

Italic numbers 1–16 correspond to the analyses shown on Fig. 5.

## Discussion

### *Refined composition of Vishteritsa columbite*

The new EPMA and LA-ICP-MS data for the major, minor and trace elements in the Vishteritsa columbite are in agreement with former data (Breskovska 1962; Yordanov et al. 1962; Arnaudov & Petrusenko, 1967) for its general composition and affiliation to the columbite-group minerals. The refined formula for the small crystal fragment based on thirteen EPMA analyses $(Mn_{0.554}Fe_{0.427}U_{0.006})_{0.987}(Nb_{1.826}Ta_{0.085}Ti_{0.116}W_{0.003})_{2.03}O_6$ defines the mineral as columbite-(Mn). This composition is characteristic for the small crystal fragment and may vary slightly in the studied crystal, as can be concluded from the LA–ICP–MS data.

The main chemical variations of the studied Vishteritsa columbite crystals are shown in Fig. 8 and might be described by the compositional variations involving either single-site substitutions such as Nb↔Ta (Fig. 8b) or Mn↔Fe (Fig. 8c), or coupled substitution represented by the following reaction: $Nb^{5+}+Mn^{2+}\leftrightarrow Ta^{5+}+Fe^{2+}$ (Fig. 8d) and $2(Nb,Ta)^{5+}\leftrightarrow(Ti,Zr,U)^{4+}$

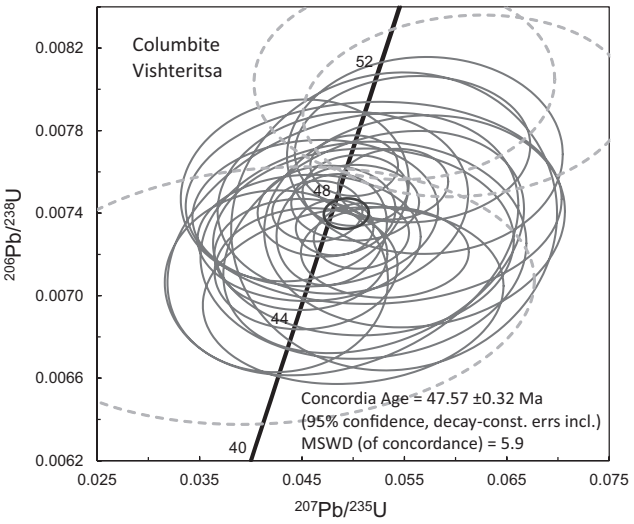


**Fig. 6.** Concordia diagram with all LA–ICP–MS U–Pb isotope data for columbite of the Vishteritsa pegmatite. The Concordia age is calculated excluding the two analyses older than 50 Ma and the single youngest analysis with high 2 sigma uncertainty (shown with dashed line).

**Table 4:** LA–ICP–MS U–Pb in-situ isotope data for zircons of granite sample Os7b from the Vishteritsa area, Western Rhodopes, Bulgaria.

| | $^{207}Pb/^{235}U$ | 2SE | $^{206}Pb/^{238}U$ | 2SE | Rho* | $^{207}Pb/^{206}Pb$ | 2SE | $^{208}Pb/^{232}Th$ | 2SE | $^{207}Pb/^{235}U$ age, Ma | 2SE | $^{206}Pb/^{238}U$ age, Ma | 2SE | Approx U_ppm | Approx Th_ppm |
|---|---|---|---|---|---|---|---|---|---|---|---|---|---|---|---|
| GrVi_1 | 0.052 | 0.009 | 0.0078 | 0.0003 | 0.017 | 0.049 | 0.009 | 0.0025 | 0.0006 | 51 | 9 | 50.3 | 1.8 | 1124 | 116 |
| GrVi_2 | 0.074 | 0.036 | 0.0081 | 0.0008 | 0.105 | 0.116 | 0.068 | 0.0030 | 0.0009 | 65 | 34 | 51.8 | 5.2 | 295 | 97 |
| GrVi_3 | 0.056 | 0.005 | 0.0085 | 0.0002 | 0.168 | 0.046 | 0.004 | 0.0027 | 0.0003 | 55 | 5 | 54.8 | 1.2 | 3280 | 402 |
| GrVi_4 | 0.058 | 0.010 | 0.0080 | 0.0003 | 0.067 | 0.054 | 0.009 | 0.0024 | 0.0003 | 57 | 9 | 51.5 | 1.9 | 2170 | 433 |
| GrVi_5 | 0.059 | 0.027 | 0.0084 | 0.0007 | 0.011 | 0.066 | 0.035 | 0.0023 | 0.0006 | 53 | 26 | 53.7 | 4.2 | 358 | 81 |
| GrVi_6 | 0.058 | 0.011 | 0.0081 | 0.0003 | 0.007 | 0.052 | 0.010 | 0.0032 | 0.0006 | 56 | 10 | 52.1 | 1.8 | 1030 | 168 |
| GrVi_7 | 0.058 | 0.011 | 0.0083 | 0.0004 | 0.042 | 0.053 | 0.011 | 0.0025 | 0.0009 | 56 | 10 | 53.4 | 2.3 | 1153 | 81 |
| GrVi_8 | 0.071 | 0.016 | 0.0088 | 0.0006 | 0.005 | 0.059 | 0.014 | 0.0028 | 0.0006 | 69 | 15 | 56.5 | 3.8 | 1070 | 228 |
| GrVi_9 | 0.063 | 0.031 | 0.0081 | 0.0007 | 0.043 | 0.055 | 0.045 | 0.0020 | 0.0010 | 53 | 29 | 52.0 | 4.7 | 172 | 58 |
| GrVi_10 | 0.058 | 0.007 | 0.0089 | 0.0002 | 0.054 | 0.048 | 0.006 | 0.0030 | 0.0007 | 57 | 7 | 56.8 | 1.4 | 2335 | 128 |
| GrVi_11 | 0.066 | 0.015 | 0.0084 | 0.0004 | 0.112 | 0.057 | 0.013 | 0.0030 | 0.0005 | 63 | 14 | 53.6 | 2.7 | 1010 | 216 |
| Os7bD_1 | 0.052 | 0.003 | 0.0078 | 0.0001 | 0.056 | 0.048 | 0.003 | 0.0024 | 0.0001 | 51 | 3 | 50.1 | 0.6 | 3170 | 598 |
| Os7bD_2 | 0.057 | 0.003 | 0.0083 | 0.0001 | 0.157 | 0.049 | 0.003 | 0.0023 | 0.0002 | 56 | 3 | 53.1 | 0.8 | 3894 | 445 |
| Os7bD_3 | 0.056 | 0.014 | 0.0072 | 0.0003 | 0.037 | 0.059 | 0.016 | 0.0019 | 0.0003 | 52 | 13 | 46.0 | 2.1 | 504 | 220 |
| Os7bD_4 | 0.056 | 0.015 | 0.0073 | 0.0003 | 0.053 | 0.056 | 0.016 | 0.0020 | 0.0003 | 55 | 14 | 46.7 | 2.2 | 582 | 257 |
| Os7bD_5 | 0.051 | 0.014 | 0.0080 | 0.0004 | 0.003 | 0.044 | 0.013 | 0.0025 | 0.0006 | 47 | 13 | 51.3 | 2.5 | 568 | 98 |
| Os7bD_6 | 0.054 | 0.004 | 0.0082 | 0.0001 | 0.042 | 0.048 | 0.004 | 0.0021 | 0.0001 | 53 | 4 | 52.8 | 0.8 | 3900 | 1015 |
| Os7bD_7 | 0.052 | 0.007 | 0.0079 | 0.0002 | 0.003 | 0.049 | 0.007 | 0.0026 | 0.0004 | 49 | 7 | 50.5 | 1.2 | 788 | 122 |
| Os7bD_8 | 0.153 | 0.005 | 0.0225 | 0.0002 | 0.081 | 0.050 | 0.002 | 0.0065 | 0.0002 | 144 | 4 | 143 | 1.2 | 2586 | 923 |
| Os7bD_9 | 0.056 | 0.006 | 0.0084 | 0.0002 | 0.047 | 0.047 | 0.005 | 0.0023 | 0.0003 | 55 | 6 | 53.8 | 1.1 | 2811 | 349 |
| Os7bD_10 | 0.078 | 0.017 | 0.0111 | 0.0005 | 0.029 | 0.050 | 0.011 | 0.0041 | 0.0006 | 72 | 15 | 71.1 | 3.3 | 386 | 93 |
| Os7bD_11 | 0.061 | 0.020 | 0.0076 | 0.0004 | 0.032 | 0.066 | 0.025 | 0.0030 | 0.0004 | 51 | 18 | 48.9 | 2.6 | 214 | 120 |
| Os7bD_12 | 0.054 | 0.020 | 0.0080 | 0.0004 | 0.007 | 0.051 | 0.021 | 0.0028 | 0.0006 | 48 | 19 | 51.5 | 2.9 | 237 | 73 |
| Os7bD_13 | 0.038 | 0.027 | 0.0079 | 0.0005 | 0.046 | 0.036 | 0.049 | 0.0030 | 0.0007 | 16 | 25 | 50.4 | 3.4 | 103 | 43 |
| Os7bD_14 | 0.047 | 0.013 | 0.0077 | 0.0003 | 0.035 | 0.045 | 0.012 | 0.0021 | 0.0004 | 48 | 13 | 49.4 | 2.2 | 571 | 212 |
| Os7bD_15 | 0.055 | 0.017 | 0.0079 | 0.0004 | 0.143 | 0.046 | 0.018 | 0.0024 | 0.0005 | 47 | 16 | 50.4 | 2.4 | 268 | 77 |

* Rho = error correlation of $^{206}Pb/^{238}U - ^{207}Pb/^{235}U$

$+(W)^{6+}$ (Fig. 8f) (Ercit 1994; Melcher et al. 2015). The plot of tetravalent versus pentavalent cations (Fig. 8e) suggest a euxenite-type substitution, resulting in ordering of Ti at the *B* site (approx. 1:1 distribution; Ercit 1994). These substitutions are inferred for the crystal parts away from cracks and inclusions (analyses for points 11–16 on Fig. 5a). In altered parts of the columbite the trends become obscure (Fig. 8b–f, analyses 1–9 marked with crosses) and suggest mobility of some elements during overprinting hydrothermal processes.

The variation of the major (Ta, Mn, Ti) and some minor elements like Zr, W, U and Zn between the analytical points (Fig. 9a) reveal the similar behaviour of Ti, Zr, U and W that was concluded from the possible substitution mechanisms in the Vishteritsa columbite. Our study confirms the high uranium content of the Vishteritsa columbite that attains up to 0.8 wt. % $UO_2$. However, in outer and porous parts and proximal to cracks there is a substantial decrease of its content below 0.2 wt. %, which infers the mobility of this element during overprinting fluid-induced processes. The latter can explain the observations of uraninite Breskovska (1962) and Yordanov et al. (1962) and possibly other secondary uranium minerals (Fig. 5b–d) that finely penetrate cracks and replace the columbite.

The LREE content in the Vishteritsa columbite is very low (often below the limits of detection with the applied techniques) and the mineral is enriched in HREE (306–697 ppm). The sums of REE (LREE+HREE) in the range 356–733 ppm define the studied columbite as moderately REE-enriched, compared with columbites from other regions of the world (e.g., summaries of Graupner et al. 2010 and Siachoque et al. 2020). Chondrite-normalized REE patterns of the Vishteritsa columbite are characterized by steep increase of the normalized values from the LREE to the middle (M) and HREE and moderate increase from MREE to HREE with a deep Eu anomaly. This signature should be explained by fractionation of light to middle REE-bearing minerals (allanite, titanite, apatite, monazite) during the granite and pegmatite fractionation and before the start of columbite crystallization. The deep Eu-anomaly (Eu below the detection limit) on the chondrite-normalized patterns (Fig. 9b) also argues for crystallization from highly fractionated magma and fluid-rich melt, after the fractionation of plagioclase and other Ca-rich minerals (e.g., London 2008; Černý et al. 2012).

### *Age of the Vishteritsa pegmatites and their relationship to the RWRB granitoids*

The LA–ICP–MS U–Pb results show that this technique is a perfect tool to apply for columbite and pegmatite dating using a matrix-matched SRM. In this case, we used a quadrupole ICP–MS and columbite X36 SRM dated previously with the conventional ID–TIMS method (von Quadt et al. 2019; Galliski et al. 2021). Both, the SRM and the studied Vishteritsa columbite behave similarly during laser ablation; consequently,

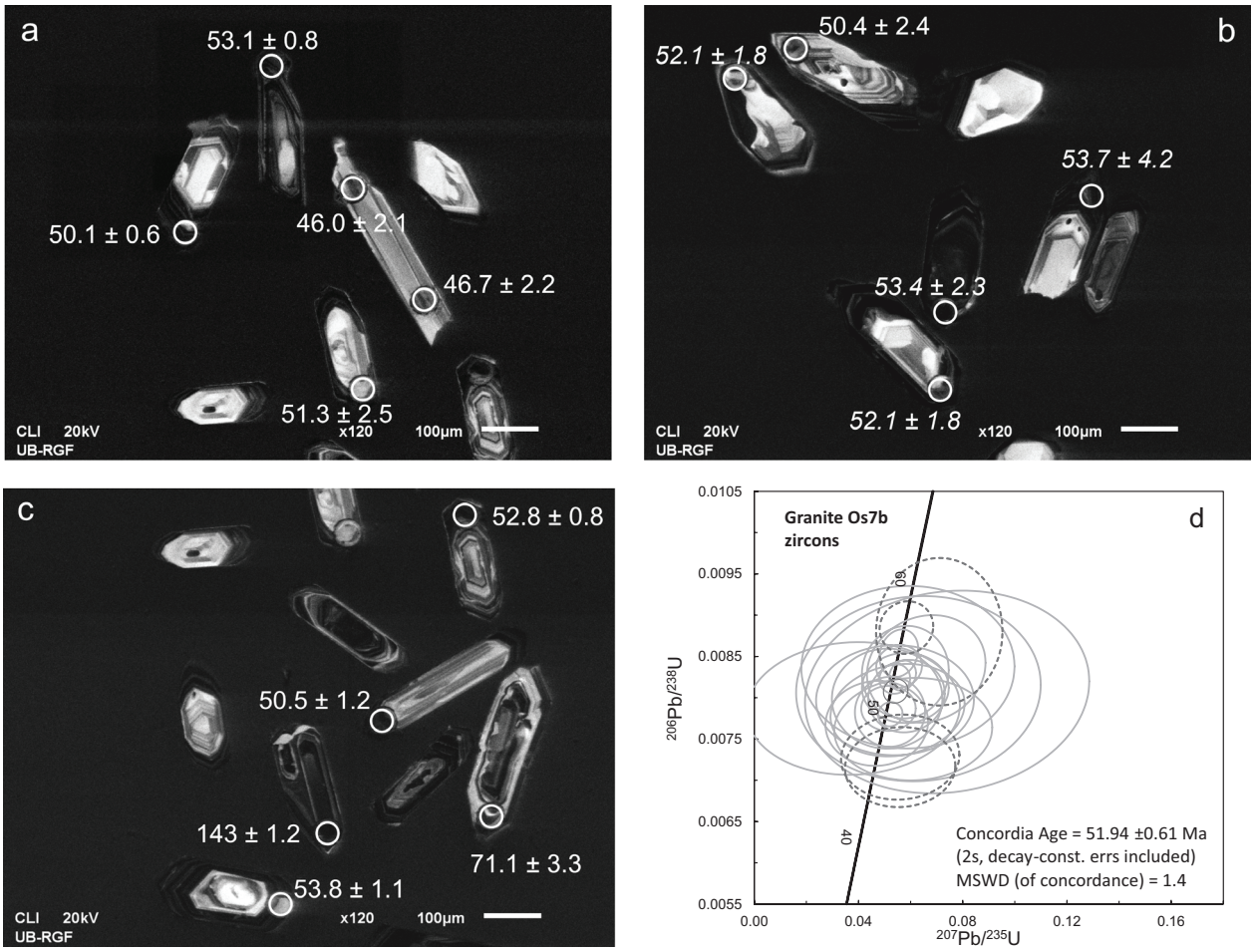


**Fig. 7.** Cathode-luminescent images of zircons from Os7b granite sample (**a**, **b** and **c**) with the position of the laser-ablation craters and the corresponding $^{206}Pb/^{238}U$ ages in Ma, and the Concordia diagram for all zircons (**d**); outlier analyses are shown with dashed line and excluded from the calculations.

the applied down-hole fractionation correction (algorithm of Paton et al. 2011) resulted in reliable age data. The individual columbite U–Pb ages are concordant and with usual uncertainty less than 5 % (usually less than 3 %) for the best measured $^{206}Pb/^{238}U$ ratios. They encourage the potential application of this technique and SRMs for dating of similar type of deposits all over the world.

The obtained columbite Concordia age of 47.57±0.32 Ma (with spread of individual $^{206}Pb/^{238}U$ ages between 45 and 51.3 Ma) is in agreement with earlier isotope dating of the Vishteritsa pegmatites by U–Pb method on zircon (50±5 Ma; Arnaudov et al. 1969) or by K–Ar on muscovite (around 50 Ma; Boyadzhiev & Lilov 1976). Pegmatites are younger than the 68–71 Ma Late Cretaceous granites of RWRB (Peytcheva et al. 2007; Stavrev et al. 2020) but also are older than the ~40 Ma old Late Paleogene granites of the batholith (Peytcheva et al. 1998, 2007). This discrepancy is solved with our new in situ U–Pb zircon dating of the granite that hosts the columbite-bearing pegmatite at 51.94±0.61 Ma. The Vishteritsa rare-element granitic pegmatites should be related to these Early Eocene granites that cover a wide area south of the Babyak–Grashevo shear zone (Fig. 2). The slightly younger age of the columbite from Vishteritsa pegmatite is possibly related to Pb-loss during overprinting hydrothermal processes, if we have in mind the spatial variations in the U-content, the observations of Breskovska et al. (1962) and Yordanov et al. (1962) and our own data for the secondary uranium minerals in cracks of the columbite. Evidence for the hydrothermal alteration and replacement of earlier pegmatite associations by later quartz–albite–muscovite association were also described by former researchers of the pegmatite (Ivanov 1991). These fluids are probably late-magmatic and exsolved from the residual melt and/or locally mixed with external fluids derived from the host rocks during the Late Eocene–Oligocene (ca. 40 Ma) magmatism; the presence of volatiles (mainly $H_2O$, F) facilitates high mobility of the elements and the replacement processes (e.g., Chládek et al. 2020). However, we should not absolutely exclude an (additional) possibility for episodic protracted growth history of pegmatites and columbite, as was suggested for high-pressure (miaskite-type) pegmatites in the Ivrea zone of the Alps (Schaltegger et al. 2015).

The newly measured granite age infers a more complex character of the RWRB and a possibility of incremental episodic growth over a long period (~70 to ~40 Ma), as was observed in collisional to post-collisional plutons in the Alpine–Himalayan Belt (e.g., Rezeau et al. 2016). Current reliable U–Pb zircon age dating of the RWRB argues for magmatic episodes at ~70 Ma and 42–39 Ma (Kamenov et al. 1999; Peytcheva et al. 2007; Stavrev et al. 2020) and they are complemented with the new 51.94±0.61 Ma old granite ages in the Vishteritsa area. Although it is not easy to distinguish granites of different age in the field, the compositional characteristics of the Eocene granites allow us to assume their wide distribution south of the Babyak–Grashevo shear zone (Fig. 2).

Cenozoic granitoid magmatism accompanied by pegmatites in the Rhodopes covers a wider age range from ~58 to 42 Ma (Marchev et al. 2013). In the Middle Allochthone of the Rhodopes, which is the metamorphic frame of RWRB, the closest pegmatites and granitoids are dated to 48–52 Ma (Gorinova et al. 2019) NNE of the batholith (in the Rila Mountain), and to ~56 Ma (Kapatnik pluton, Rila Mountain, Milovanov et al. 2010; Dolno Dryanovo, Western Rhodopes and Spanchevtsi, Pirin Mountain; Jahn-Awe et al. 2010) (Fig. 1; see also Marchev et al. 2013). Additional dating in the western and southern parts of the RWRB is needed for better constraints of the link between columbite-bearing rare-element pegmatites and the Eocene granitoid magmatism.

Many of the Early to Middle Eocene granitoid intrusives reveal adakite-like signatures resulting from high-pressure amphibole fractionation accompanied by trace-element rich accessory minerals and water suppressed plagioclase fractionation. Our preliminary unpublished geochemical data for the Early Eocene granite in the Vishteritsa pegmatite region allow us to refer them to the same group of adakite-like granitoids. Mantle underplating and interaction with the mid- to lower part of collision- and underplating-induced thickened crust in the Rhodopes are suggested to explain the favourable conditions for their formation (Marchev et al. 2013). The evidence for an ongoing collision in the lower part of the nappe system of the RMC (Georgiev et al. 2010; Jahn-Awe et al. 2010, 2012; Gautier et al. 2017; Gorinova et al. 2019) are an additional option that will result in the stacking of magmas in the lower part of the thickened crust. This process may lead to water saturation and high-pressure fractionation of amphibole and trace-element rich accessory minerals and may result in adakitic magma that is potentially fertile for some ore deposits (Chiaradia 2009; Richards 2011). The affiliation of the southern part of the RWRB to the group of adakite-like plutons may be used as a possible tool to estimate its economic potential as a source of conventional and strategic rare metals.

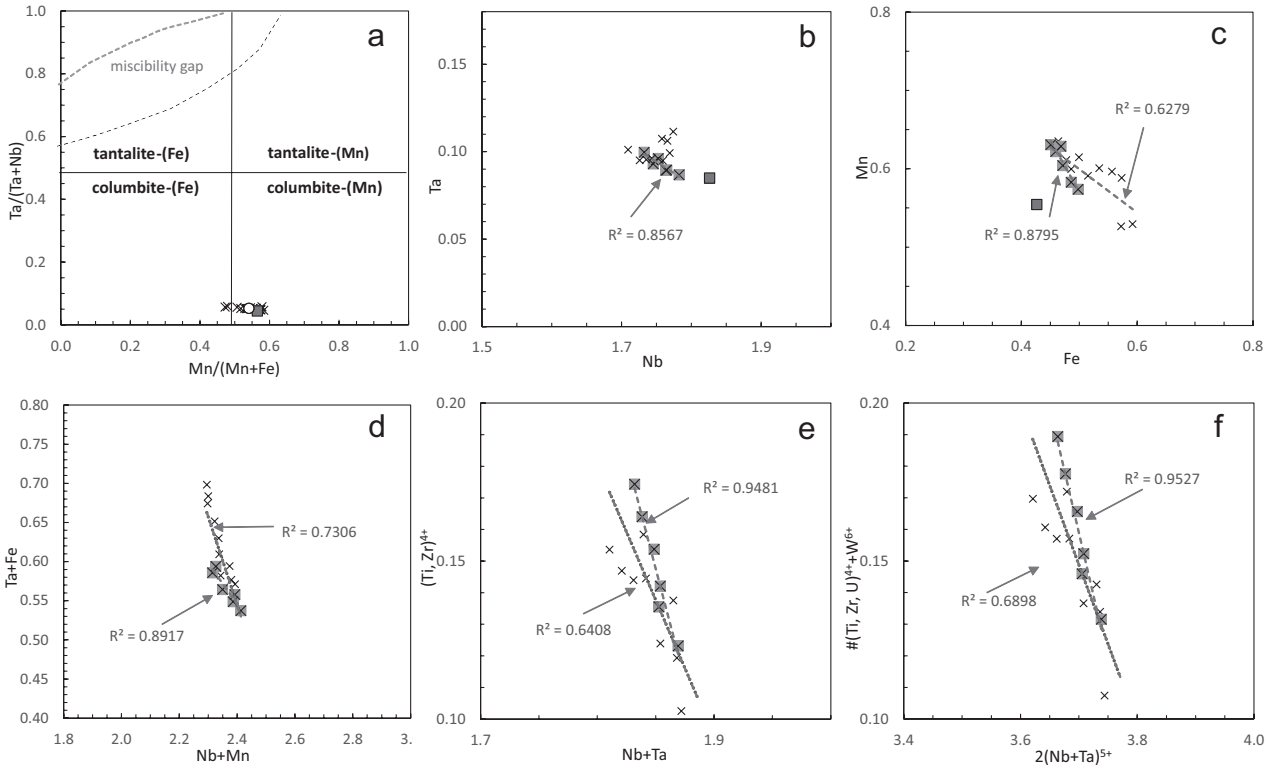


**Fig. 8.** Compositional variations in the columbite from the Vishteritsa pegmatite. **a** — Quadrilateral diagram (e.g. Černý & Ercit 1989) defining the studied columbite fragment as columbite-(Mn); the grey square shows the average composition based on thirteen EPMA analyses of the unaltered part of the crystal, and the white circle an average of the LA–ICP–MS analyses (crosses); **b–f:** Nb vs Ta (b), Fe vs Mn (c), Nb+Mn vs Ta+Fe (d), Nb+Ta vs Ti+Zr (e), and 2(Nb+Ta) vs (Ti, Zr, U)+W (f) plots (the squares with crosses are used for analyses 11–16 in Table 5 corresponding to unaltered parts away from cracks).

**Table 5:** LA–ICP–MS analyses of columbite from Vishteritsa pegmatite, Western Rhodopes (for the position of the analytical spots see Fig. 5a). The values with "<" correspond to the limit of detection for these elements and are used for the plot on Fig. 8b.

| Analysis | 1 | 2 | 3 | 4 | 5 | 6 | 7 | 8 | 9 | 10 | 11 | 12 | 13 | 14 | 15 | 16 | average |
|---|---|---|---|---|---|---|---|---|---|---|---|---|---|---|---|---|---|
| $WO_3$ | 0.13 | 0.33 | 0.23 | 0.23 | 0.23 | 0.25 | 0.21 | 0.22 | 0.11 | 0.23 | 0.17 | 0.21 | 0.20 | 0.23 | 0.32 | 0.24 | 0.22 |
| $Nb_2O_5$ | 67.64 | 65.36 | 66.14 | 66.57 | 67.17 | 67.50 | 67.79 | 67.53 | 67.90 | 67.10 | 68.79 | 67.95 | 68.09 | 67.30 | 66.73 | 67.54 | 67.32 |
| $Ta_2O_5$ | 6.76 | 6.43 | 6.06 | 6.09 | 6.04 | 6.05 | 6.32 | 6.86 | 7.09 | 6.15 | 5.57 | 5.72 | 5.74 | 5.96 | 6.38 | 6.16 | 6.21 |
| $TiO_2$ | 2.15 | 3.16 | 3.04 | 2.97 | 3.02 | 2.56 | 2.40 | 2.60 | 2.02 | 3.29 | 2.62 | 2.86 | 3.02 | 3.45 | 3.67 | 3.24 | 2.88 |
| $UO_2$ | 0.23 | 0.87 | 0.80 | 0.75 | 0.71 | 0.69 | 0.89 | 0.14 | 0.28 | 0.79 | 0.47 | 0.57 | 0.57 | 0.80 | 0.81 | 0.66 | 0.63 |
| FeO | 12.26 | 11.85 | 11.53 | 11.08 | 10.70 | 10.36 | 9.89 | 9.63 | 11.84 | 10.11 | 9.40 | 9.76 | 9.58 | 9.83 | 10.12 | 10.37 | 10.52 |
| MnO | 10.83 | 12.01 | 12.20 | 12.30 | 12.13 | 12.59 | 12.50 | 13.03 | 10.76 | 12.32 | 12.99 | 12.93 | 12.81 | 12.43 | 11.98 | 11.80 | 12.22 |
| Total | 100.0 | 100.0 | 100.0 | 100.0 | 100.0 | 100.0 | 100.0 | 100.0 | 100.0 | 100.0 | 100.0 | 100.0 | 100.0 | 100.0 | 100.0 | 100.0 | 100.0 |
| *Formula calculated to 6 atoms of O* | | | | | | | | | | | | | | | | | |
| Fe | 0.592 | 0.573 | 0.556 | 0.534 | 0.515 | 0.500 | 0.478 | 0.464 | 0.572 | 0.486 | 0.451 | 0.468 | 0.459 | 0.472 | 0.486 | 0.498 | 0.506 |
| Mn | 0.529 | 0.588 | 0.597 | 0.601 | 0.591 | 0.615 | 0.611 | 0.635 | 0.526 | 0.600 | 0.631 | 0.629 | 0.622 | 0.604 | 0.583 | 0.574 | 0.596 |
| U | 0.003 | 0.011 | 0.010 | 0.010 | 0.009 | 0.009 | 0.011 | 0.002 | 0.004 | 0.010 | 0.006 | 0.007 | 0.007 | 0.010 | 0.010 | 0.008 | 0.008 |
| *A site total* | 1.125 | 1.173 | 1.163 | 1.145 | 1.115 | 1.123 | 1.100 | 1.101 | 1.102 | 1.096 | 1.087 | 1.104 | 1.088 | 1.086 | 1.079 | 1.080 | 1.11 |
| Nb | 1.766 | 1.709 | 1.726 | 1.735 | 1.747 | 1.759 | 1.769 | 1.758 | 1.774 | 1.743 | 1.782 | 1.763 | 1.765 | 1.745 | 1.732 | 1.753 | 1.752 |
| Ta | 0.106 | 0.101 | 0.095 | 0.096 | 0.094 | 0.095 | 0.099 | 0.107 | 0.111 | 0.096 | 0.087 | 0.089 | 0.090 | 0.093 | 0.100 | 0.096 | 0.097 |
| Ti | 0.094 | 0.138 | 0.132 | 0.129 | 0.131 | 0.111 | 0.104 | 0.113 | 0.088 | 0.142 | 0.113 | 0.124 | 0.130 | 0.149 | 0.158 | 0.140 | 0.125 |
| W | 0.002 | 0.005 | 0.003 | 0.003 | 0.003 | 0.004 | 0.003 | 0.003 | 0.002 | 0.003 | 0.003 | 0.003 | 0.003 | 0.003 | 0.005 | 0.003 | 0.003 |
| *B site total* | 1.967 | 1.953 | 1.956 | 1.963 | 1.976 | 1.969 | 1.976 | 1.981 | 1.975 | 1.985 | 1.985 | 1.979 | 1.987 | 1.991 | 1.995 | 1.992 | 1.977 |
| *Mn/(Mn + Fe)* | 0.472 | 0.506 | 0.517 | 0.529 | 0.534 | 0.552 | 0.561 | 0.578 | 0.479 | 0.552 | 0.583 | 0.573 | 0.575 | 0.562 | 0.545 | 0.535 | 0.541 |
| *Ta/(Ta + Nb)* | 0.057 | 0.056 | 0.052 | 0.052 | 0.051 | 0.051 | 0.053 | 0.058 | 0.059 | 0.052 | 0.046 | 0.048 | 0.048 | 0.051 | 0.054 | 0.052 | 0.053 |
| *Trace elements, ppm* | | | | | | | | | | | | | | | | | |
| Sc | 65 | 81 | 63 | 62 | 64 | 50 | 57 | 57 | 64 | 63 | 50 | 62 | 59 | 62 | 66 | 54 | 61 |
| Zn | 783 | 647 | 680 | 694 | 660 | 481 | 417 | 543 | 1097 | 662 | 596 | 635 | 545 | 529 | 468 | 514 | 622 |
| Y | 428 | 483 | 456 | 486 | 451 | 578 | 837 | 278 | 374 | 460 | 420 | 422 | 430 | 448 | 456 | 429 | 465 |
| Zr | 2434 | 4261 | 3952 | 3850 | 3748 | 3437 | 4103 | 6755 | 1456 | 4131 | 2560 | 3072 | 3202 | 3896 | 4156 | 3750 | 3673 |
| Sn | 32 | 49 | 50 | 42 | 35 | 26 | 27 | 49 | 16 | 59 | 29 | 36 | 27 | 48 | 51 | 40 | 38 |
| La | <0.60 | <0.94 | <1.56 | <1.32 | <1.27 | <1.15 | <1.25 | <1.96 | 2.06 | <1.08 | <0.90 | <0.68 | <0.93 | <0.79 | <1.08 | <0.91 | 2.06 |
| Ce | <0.89 | <0.98 | <1.63 | <1.39 | <1.34 | <1.20 | <1.32 | <1.49 | 25.09 | 1.32 | <0.96 | <0.73 | <0.99 | 1.30 | <1.16 | <0.97 | 9.24 |
| Pr | <0.48 | <0.75 | <1.25 | <1.06 | <1.02 | <0.92 | 1.10 | <1.14 | 0.90 | <0.87 | <0.73 | <0.55 | <0.75 | <0.64 | <0.88 | <0.74 | 1.00 |
| Nd | <3.16 | <4.91 | <8.16 | <6.94 | <6.66 | <5.99 | 9.54 | <7.41 | <5.61 | <5.66 | 4.59 | <3.45 | <4.73 | <4.05 | <5.52 | <4.63 | 7.06 |
| Sm | 9.64 | 16.27 | 13.17 | 8.99 | 7.42 | 10.91 | 25.66 | 8.26 | 7.12 | 9.15 | 5.17 | 9.61 | 6.14 | 12.90 | 14.91 | 9.64 | 11 |
| Eu | <1.06 | <1.65 | <2.74 | <2.33 | <2.23 | <2.01 | <2.20 | <2.49 | <1.88 | <1.90 | <1.57 | <1.19 | <1.62 | <1.39 | <1.89 | <1.59 | <1.2 |
| Gd | 20.4 | 38.9 | 29.6 | 30.4 | 30.0 | 43.0 | 66.1 | 8.7 | 17.9 | 33.8 | 23.7 | 29.0 | 20.3 | 27.7 | 38.2 | 22.8 | 30 |
| Tb | 11.3 | 13.6 | 15.3 | 15.6 | 13.2 | 19.3 | 26.9 | 5.2 | 12.3 | 12.9 | 12.0 | 12.6 | 12.3 | 12.8 | 10.8 | 10.4 | 14 |
| Dy | 85 | 113 | 92 | 93 | 107 | 121 | 207 | 44 | 82 | 99 | 90.3 | 86.3 | 101 | 97.8 | 104 | 94.9 | 101 |
| Ho | 19.5 | 18.4 | 19.0 | 18.0 | 15.9 | 21.9 | 28.0 | 9.5 | 16.9 | 15.2 | 13.7 | 17.1 | 13.5 | 14.6 | 15.1 | 15.0 | 17 |
| Er | 60 | 59 | 62 | 57 | 54 | 74 | 110 | 42 | 67 | 62 | 48.1 | 49.8 | 53.0 | 60.1 | 45.0 | 53.0 | 60 |
| Tm | 13.9 | 12.4 | 12.8 | 11.7 | 11.2 | 15.7 | 21.1 | 12.6 | 15.0 | 15.1 | 10.3 | 11.6 | 12.2 | 11.9 | 12.8 | 12.7 | 13 |
| Yb | 148 | 150 | 147 | 124 | 118 | 143 | 205 | 158 | 126 | 131 | 113 | 125 | 119 | 121 | 116 | 115 | 135 |
| Lu | 21.5 | 18.0 | 21.1 | 22.4 | 17.7 | 24.9 | 32.2 | 26.4 | 24.1 | 18.6 | 18.7 | 17.8 | 17.8 | 19.8 | 16.7 | 17.6 | 21 |
| Hf | 201 | 437 | 367 | 391 | 366 | 336 | 365 | 580 | 130 | 389 | 239 | 293 | 301 | 367 | 413 | 380 | 347 |
| Th | 9.4 | 35.2 | 31.9 | 32.2 | 29.0 | 46.1 | 96.4 | 2.3 | 50.5 | 30.9 | 19.3 | 24.2 | 21.7 | 29.0 | 31.9 | 25.2 | 32 |
| SumREE | 389 | 439 | 411 | 381 | 374 | 473 | 733 | 314 | 396 | 398 | 340 | 359 | 356 | 380 | 374 | 351 | 404 |

*Crystal chemical formula of columbite from Vishteritsa pegmatite, Western Rhodopes based on 16 LA–ICP–MS analyses* $(Mn_{0.596}Fe_{0.506}U_{0.008})_{1.11}\ (Nb_{1.752}Ta_{0.097}Ti_{0.125}W_{0.003})_{1.977}\ O_6$

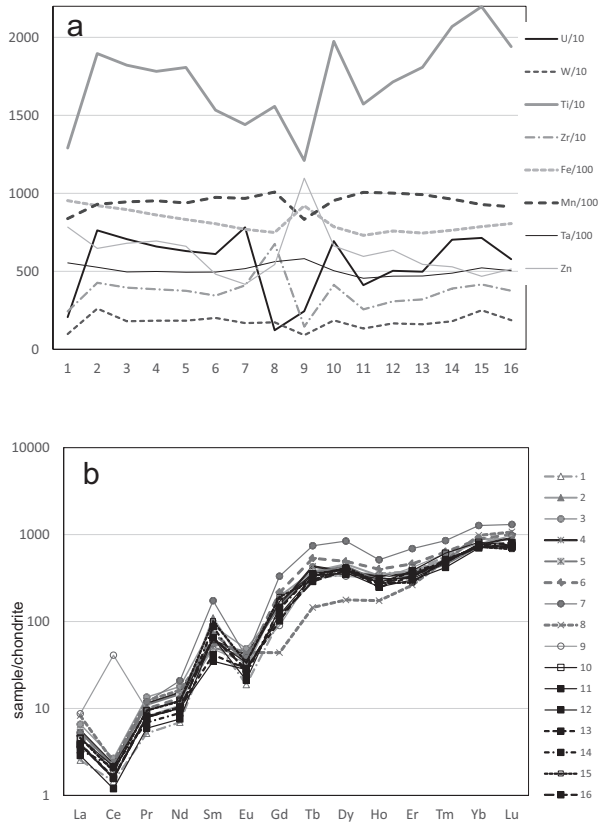


**Fig. 9.** Geochemical diagrams for the Vishteritsa columbite. **a** — Variation of Ta, Mn, Fe, Ti , U, Zr and W in the columbite (LA–ICP–MS data for point analyses 1–16, Fig. 5a and Table 5); **b** — Chondrite C1 (McDonough & Sun 1995) normalized REE patterns for the Vishteritsa columbite; analyses of the unaltered fragments of the crystal (10–16) are shown in black, others (1–9) in grey.

## Conclusions

- The first U–Pb LA–ICP–MS dating of columbite from the Vishteritsa pegmatite defines Early Eocene age 47.57± 0.32 Ma (with spread of individual $^{206}Pb/^{238}U$ ages between 45 and 51.3 Ma).
- Based on the EPMA data for the composition the refined formula of the mineral $(Mn_{0.554}Fe_{0.427}U_{0.006})_{0.987}(Nb_{1.826}Ta_{0.085}Ti_{0.116}W_{0.003})_{2.03}O_6$ classifies it as columbite-(Mn).
- The typical trace elements of the columbite from the Vishteritsa rare-element pegmatites are Ti, U, Zr, W, Y, Hf and Zn and their fluctuation trends are linked to possible substitution mechanisms or interpreted by mobility during fluid-induced processes.
- The Vishteritsa columbite is relatively rich in REE and reveals a chondrite-normalized pattern with clear HREE enrichment and deep Eu-anomaly. They argue for crystallization from highly fractionated fluid-rich magma.
- High $UO_2$ content reaching 0.8 wt. % is characteristic for the Vishteritsa columbite. Lower uranium content proximal to cracks and in outer crystal zones documents U-mobility during overprinting hydrothermal processes.
- The rare metal pegmatites are related to Early Eocene granite magmatism, dated at 51.94±0.61 Ma in the area of rare-element pegmatites (with spread of individual $^{206}Pb/^{238}U$ ages mainly between 49 Ma and 53 Ma). This age infers episodic growth of the RWRB over more than 30 Ma (71–39 Ma) and it defines the Early Eocene granite magmatism as fertile.

**Acknowledgements:** The authors thank the National Museum of Natural History staff (Chavdar Karov and Iliya Dimitrov) for providing a fragment of a museum specimen for the current study. The study is partly financially supported by an SEG student grant and KP-06-N34/4 project of the Bulgarian National Science Fund to MS.

## References

Arnaudov V. & Petrusenko S. 1967: Primary accessory mineralization in the pegmatites from the Vishteritsa locality, Western Rhodopes. *Bulletin of the Geological Institute Series Geochemistry, Mineralogy and Petrography* 16, 145–157 (in Bulgarian).

Arnaudov V., Amov B. & Pavlova M. 1969: On the absolute geological age of certain pegmatites in South Bulgaria. *Bulletin of the Geological Institute, Series Geochemistry, Mineralogy and Petrology* 18, 19–27 (in Bulgarian with English abstract).

Baumgartner R., Romer R.L., Moritz R., Sallet R. & Chiaradia M. 2006: Columbite–tantalite–bearing granitic pegmatites from the Seridó Belt, northeastern Brazil: genetic constraints from U–Pb dating and Pb isotopes. *Canadian Mineralogist* 44, 69–86. https://doi.org/10.2113/gscanmin.44.1.69

Bonev N. & Stampfli G. 2008: Petrology, geochemistry and geodynamic implications of Jurassic island arc magmatism as revealed by mafic volcanic rocks in the Mesozoic low-grade sequence, eastern Rhodope, Bulgaria. *Lithos* 100, 210–233. https://doi.org/10.1016/j.lithos.2007.06.019

Bonev N., Burg J.-P. & Ivanov Z. 2006: Mesozoic-Tertiary structural evolution of an extensional gneiss dome – the Kesebir–Kardamos dome, eastern Rhodope (Bulgaria–Greece). International Journal of Earth Sciences 95, 318–340. https://doi.org/10.1007/s00531-005-0025-y

Bosse V., Boulvais P., Gautier P., Tiepolo M., Ruffet J., Devidal L., Cherneva Z., Gerdjikov I. & Paquette J. 2009: Fluid-induced disturbance of the monazite Th-Pb chronometer: in situ dating and element mapping in pegmatites from the Rhodopes (Greece, Bulgaria). *Chemical Geology* 261, 286–302. https://doi.org/10.1016/j.chemgeo.2008.10.025

Boyadzhiev S. & Lilov P. 1976: About the K–Ar data for South-Bulgarian granites from the West Rhodopean Block and the Krashtides. *Journal of the Bulgarian Geological Society* 37, 161–169 (in Bulgarian with English abstract).

Breskovska V. 1962: Studies on columbite from the Rhodope and Sredna Gora mountain. *Annual of Sofia University "St. Kliment Ohridski" Faculty of Biology, Geology and Geography* 55, Book 2 Geology, 191–198 (in Bulgarian).

Burg J.-P. 2012: Rhodope: from Mesozoic convergence to Cenozoic extension. Review of petro-structural data in the geochronological frame. In: Skourtos E. & Lister G.S. (Eds.): The Geology of Greece. *Journal of the Virtual Explorer* 42, 1–44. https://doi.org/10.3809/jvirtex.2011.00270

Burg, J.-P., Ivanov Z., Ricou L.-E., Dimov D. & Klain L. 1990: Implications of shear-sense criteria for the tectonic evolution of the central Rhodope Massif, southern Bulgaria. *Geology* 18,

451–454. https://doi.org/10.1130/0091-7613(1990)018%3C0451:IOSSCF%3E2.3.CO;2

Burg J.-P., Ricou L.-E., Ivanov Z., Godfriaux I., Dimov D., Klain L. 1996: Syn-metamorphic nappe complex in the Rhodope Massif: Structure and kinematics. *Terra Nova* 8, 6–15. https://doi.org/10.1111/j.1365-3121.1996.tb00720.x

Černý P. (Ed.) 1982: Granitic pegmatites in science and industry. *Mineralogical Association of Canada Short Course Handbook* 8, 1–555.

Černý P. & Ercit T.S. 1989: Mineralogy of niobiumand tantalum: crystal chemical relationships, paragenetic aspects and their economic implications. In: Möller P., Černý F. & Saupé F. (Eds.): Lanthanides, Tantalum and Niobium. *Springer,* Berlin, 27–79.

Černý P. & Ercit T.S. 2005. The classification of granitic pegmatites revisited. *Canadian Mineralogist* 43, 2005–2026.

Černý P., Ercit S.T., Smeds S.A., Groat L.A. & Chapman R. 2007: Zirconium and hafnium in minerals of the columbite and wodginite groups from granitic pegmatites. *Canadian Mineralogist* 45, 185–202.

Černý P., London D. & Novak M. 2012 Granitic pegmatites as reflections of their sources. *Elements* 8, 289–294.

Che X.-D., Wu F.-Y., Wang, R.-C., Gerdes A., Ji W.-Q., Zhao Z.-H., Yang, J.-H. & Zhu Z.-Y. 2015: In situ U–Pb isotopic dating of columbite-tantalite by LA-ICP-MS. *Ore Geology Reviews* 65, 979–989. https://doi.org/10.1016/j.oregeorev.2014.07.008

Che X.-D., Wang R.-Ch., Wu F.-Y., Zhu Z.-Y., Zhang W.-L., Hu H., Xie L., Lu J.-J. & Zhang D. 2019: Episodic Nb–Ta mineralization in South China: Constraints from in situ LA–ICP–MS columbite-tantalite U–Pb dating. *Ore Geology Reviews* 105, 71–85. https://doi.org/10.1016/j.oregeorev.2018.11.023

Chiaradia M. 2009: Adakite-like magmas from fractional crystallization and melting-assimilation of mafic lower crust (Eocene Macuchi arc, Western Cordillera, Ecuador). *Chemical Geology* 265, 468–487. https://doi.org/10.1016/j.chemgeo.2009.05.014

Chládek S., Uher P. & Novák M. 2020: Compositional and textural variations of columbite-group minerals from beryl–columbite pegmatites in the Maršíkov District, Bohemian Massif, Czech Republic: Magmatic versus hydrothermal evolution. *The Canadian Mineralogist* 58, 767–783. https://doi.org/10.3749/canmin.1900093

Collings D., Savov I., Maneiro K., Baxter E., Harvey J. & Dimitrov I. 2016: Late Cretaceous UHP metamorphism recorded in kyanite–garnet schists from the Central Rhodope Mountains, Bulgaria. *Lithos* 246–247, 165–181. https://doi.org/10.1016/j.lithos.2016.01.002

Deng X.D., Li J.W., Zhao X.F., Hu Z.C., Hu H., Selby D. & de Souza Z.S. 2013: U–Pb isotope and trace element analysis of columbite-(Mn) and zircon by laser ablation ICP–MS: implications for geochronology of pegmatite and associated ore deposits. *Chemical Geology* 344, 1–11. https://doi.org/10.1016/j.chemgeo.2013.02.014

Dinter D. & Royden L. 1993: Late Cenozoic extension in northeastern Greece: Strymon valley detachment system and Rhodope metamorphic core complex. *Geology* 21, 45–48.

Ercit S.T. 1994: The geochemistry and crystal chemistry of columbite-group minerals from granitic pegmatites, southwestern Grenville Province. *Canadian Mineralogist* 32, 421–438.

Froitzheim N., Jahn-Awe S., Frei D., Wainwright A.N., Maas R., Georgiev N., Nagel T.J. & Pleuger J. 2014: Age and composition of metaophiolite from the Rhodope Middle Allochthon (Satovcha, Bulgaria): a test for the maximum-allochthony hypothesis of the Hellenides. *Tectonics* 1477–1500. https://doi.org/10.1002/2014tc003526

Galliski M.A. & Černý P. 2006: Geochemistry and structural state of columbite-group minerals in granitic pegmatites of the Pampean Ranges, Argentina. *Canadian Mineralogist* 44, 645–666. https://doi.org/10.2113/gscanmin.44.3.645

Gallhofer D., von Quadt A., Peytcheva I., Schmid S. & Heinrich C. 2015: Tectonic, magmatic, and metallogenic evolution of the Late Cretaceous arc in the Carpathian-Balkan orogen. *Tectonics* 34, 1813–1836. https://doi.org/10.1002/2015TC003834

Galliski M., von Quadt A. & Márquez-Zavalía M.-F. 2021: LA-ICP-MS U-Pb columbite ages and trace-element signature from rare-element granitic pegmatites of the Pampean Pegmatite Province, Argentina. *Lithos* 386–387, 106001. https://doi.org/10.1016/j.lithos.2021.106001

Gautier P., Bosse V., Cherneva Z., Didier A., Gerdjikov I. & Tiepolo M. 2017: Polycyclic alpine orogeny in the Rhodope metamorphic complex. *Bulletin de la Société Géologique de France* 188, 36. https://doi.org/10.1051/bsgf/2017195

Georgiev N., Pleuger J., Froitzheim N., Sarov S., Jahn-Awe S. & Nagel T.J. 2010: Separate Eocene–Early Oligocene and Miocene stages of extension and core complex formation in the Western Rhodopes, Mesta Basin, and Pirin Mountains (Bulgaria). *Tectonophysics* 487, 59–84. https://doi.org/10.1016/j.tecto.2010.03.009

Gerdjikov I. 2012: Penetrative shearing in the southern part of Kapatnik pluton: possible tectonic implications. In: "GEOSCIENCES 2012". *Bulgarian Geological Society*, 105–106.

Gorinova T., Georgiev N., Cherneva Z., Naydenov K., Grozdev V. & Lazarova A. 2019: Kinematics and time of emplacement of the Upper Allochthon of the Rhodope Metamorphic Complex: evidence from the Rila Mountains, Bulgaria. *International Journal of Earth Sciences* 108, 2129–2152. https://doi.org/10.1007/s00531-019-01754-2

Graupner T., Melcher F., Gabler H.-E., Sitnikova M., Bratz H. & Bahr A. 2010: Rare earth element geochemistry of columbite-group minerals: LA-ICP-MS data. *Mineralogical Magazine* 74, 691–713. https://doi.org/10.1180/minmag.2010.074.4.691

Guillong M., Meier D., Allan M., Heinrich C. & Yardley B. 2008: SILLS: a Matlab-based program for the reduction of laser ablation ICP-MS data of homogeneous materials and inclusions. In: Sylvester P. (Ed.): Laser-Ablation-ICP-MS in the Earth Sciences, current practices and outstanding issues. *Mineralogical Association of Canada, Short Course* 29, 328–333.

Harkovska A., Yanev Y., Marchev P. 1989: General features of the Paleogene orogenic magmatism in Bulgaria. *Geologica Balcanica* 19, 37–72.

Ivanov I. 1967: Internal structure and origin of the asymmetric zoned pegmatites from Srednogorie and Vishteritsa. *Communications of the Geological Institute, Serie Geochemistry, Mineralogy and Petrology* 16, 171–187 (in Bulgarian with English abstract).

Ivanov I. 1991: The granite pegmatites in Bulgaria, *Publishing house of the Bulgarian Academy of Sciences*, Sofia, *Geologica Balcanica*, *Series Operum Singulorum* 6, 1–205.

Ivanov Z. 2017: Tectonics of Bulgaria. *"St. Kliment Ohridski" Univ. Press*, Sofia, 1–332 (in Bulgarian with English abstract).

Jahn-Awe S., Froitzheim N., Nagel T.J., Frei D., Georgiev N. & Pleuger J. 2010: Structural and geochronological evidence for Paleogene thrusting in the western Rhodopes, SW Bulgaria: elements for a new tectonic model of the Rhodope Metamorphic Province. *Tectonics* 29, TC3008. https://doi.org/10.1029/2009TC002558

Jahn-Awe S., Pleuger J., Frei D., Georgiev N., Froitzheim N. & Nagel T. 2012: Time constraints for low-angle shear zones in the Central Rhodopes (Bulgaria) and their significance for the exhumation of high-pressure rocks. *International Journal of Earth Sciences* 101, 1971–2004.

Janák M., Froitzheim N., Georgiev N., Nagel T. & Sarov S. 2011: P–T evolution of kyanite eclogite from the Pirin Mountains (SW Bulgaria): implications for the Rhodope UHP Metamorphic Complex. *Journal of Metamorphic Geology* 29, 317–332. https://doi.org/10.1111/j.1525-1314.2010.00920.x

Kaiser-Rohrmeier M., von Quadt A., Driesner T., Heinrich C., Handler R., Ovtcharova M., Ivanov Z., Petrov P., Sarov S. & Peytcheva I. 2013: Post-orogenic extension and hydrothermal ore formation: high precision geochronology of the Central Rhodopian Metamorphic Core Complex (Bulgaria-Greece). *Economic Geology* 108, 691–718.

Kamenov B., Peytcheva I., Klain L., Arsova K., Kostitsin Y. & Salnikova E. 1999: Rila-West Rhodopes Batholith: Petrological and geochemical constraints for its composite character. *Geochemistry, Mineralogy and Petrology* 36, 3–27.

Kostov-Kytin V., Karov Ch., Dimitrov I. & Nikolova R. 2020: New investigations on the columbite from Vishteritsa locality, Western Rhodopes. *Comptes Rendus de l'Acad´emie Bulgare des Sciences* 73, 657–665. https://doi.org/10.7546/CRABS.2020.05.08

Liati A. 2005: Identification of repeated Alpine (ultra) high-pressure metamorphic events by U–Pb SHRIMP geochronology and REE geochemistry of zircon: the Rhodope zone of Northern Greece. *Contributions to Mineralogy and Petrology* 150, 608–630.

Liati A. & Gebauer D. 1999: Constraining the prograde and retrograde P–T–t path of Eocene HP rocks by SHRIMP dating of different zircon domains: inferred rates of heating, burial, cooling and exhumation for central Rhodope, northern Greece. *Contributions to Mineralogy and Petrology* 135, 340–354.

Liati A., Theye T., Fanning C., Gebauer D., Rayner N. 2016: Multiple subduction cycles in the Alpine orogeny, as recorded in single zircon crystals (Rhodope zone, Greece). *Gondwana Research* 29, 199–207. https://doi.org/10.1016/j.gr.2014.11.007

London D. 2008: Pegmatites. *Canadian Mineralogist Special Publication* 10, 1–347.

Ludwig K.R. 2003: User's manual for Isoplot/Ex, version 3.00. A geochronological toolkit for Microsoft Excel. *Berkeley Geochronological Centre, Special Publication* 4, 1–70.

Lupulescu M, Chiarenzelli J., Pecha M., Singer J. & Regan S. 2018: Pegmatites: Insights from isotopic and geochemical analyses columbite-group minerals from New York. *Geosciences* 169, 1–15. https://doi.org/10.3390/geosciences8050169

Marchev P., Kaiser-Rohrmeier M., Heinrich C., Ovtcharova M., von Quadt A. & Raicheva R. 2005: 2: Hydrothermal ore deposits related to post-orogenic extensional magmatism and core complex formation: the Rhodope massif of Bulgaria and Greece. *Ore Geology Reviews* 27, 53–89.

Marchev P., Georgiev S., Raicheva R., Peytcheva I., von Quadt A., Ovtcharova M. & Bonev N. 2013: Adakitic magmatism in post-collisional setting: An example from the early–middle Eocene Magmatic Belt in Southern Bulgaria and Northern Greece. *Lithos* 180–181, 159–180. https://doi.org/10.1016/j.lithos.2013.08.024

McDonough W. & Sun S. 1995: The composition of the Earth. *Chemical Geology* 120 , 223–253. https://doi.org/10.1016/0009-2541(94)00140-4

Melcher F., Graupner T., Gäbler E., Sitnikova M., Henjes-Kunst F., Oberthür T., Gerdes A. & Dewaele S. 2015: Tantalum–(niobium–tin) mineralisation in African pegmatites and rare metal granites: Constraints from Ta–Nb oxide mineralogy, geochemistry and U–Pb geochronology. *Ore Geology Reviews* 64, 667–719. https://doi.org/10.1016/j.oregeorev.2013.09.003

Melleton J., Gloaguen E., Frei D., Novák M. & Breiter K. 2012: How are the emplacement of rare-element pegmatites, regional metamorphism and magmatism interrelated in the Moldanubian domain of the Variscan Bohemian Massif, Czech Republic? *The Canadian Mineralogist* 50, 1751–1773.

Miladinova I., Froitzheim N., Nagel T., Janák M., Georgiev N., Fonseca R., Sandmann S. & Münker C. 2018: Late Cretaceous eclogite in the Eastern Rhodopes (Bulgaria): evidence for subduction under the Sredna Gora magmatic arc. *International Journal of Earth Sciences* 107, 2083–2099. https://doi.org/10.1007/s00531-018-1589-7

Milovanov P., Petrov I., Marinova A., Ilieva E., Peytcheva I., von Quadt A. & Pristavova S. 2010: New geological and geochronological data of granitic and metamorphic rocks from SW Bulgaria. *Geologica Balcanica* 39, 256.

Naydenov K., Peytcheva I., von Quadt A., Sarov S., Kolcheva K. & Dimov D. 2013: The Maritsa strike-slip shear zone between Kostenets and Krichim towns, South Bulgaria – structural, petrographic and isotope geochronology study. *Tectonophysics* 595–596, 69–89. https://doi.org/10.1016/j.tecto.2012.08.005

Ovtcharova M., von Quadt A., Cherneva Z., Sarov S., Heinrich C., Peytcheva I. 2004: U–Pb dating of zircon and monazite from granitoids and migmatites in the core and eastern periphery of the Central Rhodopean Dome, Bulgaria. *Geochimica Cosmochimica Acta* 68, A664.

Paton C., Hellstrom J., Paul B.,Woodhead J. & Hergt J. 2011: Iolite: freeware for the visualisation and processing of mass spectrometric data. *Journal of Analytical Atomic Spectrometry* 26, 2508–2518. https://doi.org/10.1039/C1JA10172B

Peytcheva I. & von Quadt A. 1995: U–Pb zircon dating of metagranites from Byala Reka region in the east Rhodopes, Bulgaria. *Geological Society Greece Special Publications* 4, 637–642.

Peytcheva I., Kostitsin Y., Salnikova E., Kamenov B. & Klain L. 1998: Rb–Sr and U–Pb isotope data for the Rila–Rhodope Batholith. *Geochemistry, Mineralogy and Petrology* 35, 3–27 (in Bulgarian with English abstract).

Peytcheva I., von Quadt A., Naydenov K., Sarov S., Dimov D. & Voinova, E. 2007: U–Pb zircon–xenotime–monazite dating and Hf-isotope tracing to distinguish Cretaceous and Paleogene granitoids in the Western Rhodopes and Rila Mountain. In: "GEOSCIENCES 2007". *Bulgarian Geological Society,* 89–91.

Rezeau H., Moritz R., Wotzlaw J.-F., Tayan R., Melkonyan R., Ulianov A., Selby D., D'Abzac F.-X. & Stern R. 2016: Temporal and genetic link between incremental pluton assembly and pulsed porphyry Cu-Mo formation in accretionary orogens. *Geology* 44, 627–630. https://doi.org/10.1130/G38088.1

Richards J.P. 2011: High Sr/Y arc magmas and porphyry Cu±Mo±Au deposits: Just add water. *Economic Geology* 106, 1075–1081. https://doi.org/10.2113/econgeo.106.7.1075

Romer R.L. & Lehmann B. 1995: U–Pb columbite age of Neoproterozoic Ta–Nb mineralization in Burundi. *Economic Geology* 90, 2303–2309. https://doi.org/10.2113/gsecongeo.90.8.2303

Romer R.L. & Smeds S.A. 1997: U–Pb columbite chronology of post-kinematic Palaeoproterozoic pegmatites in Sweden. *Precambrian Research* 82, 85–99. https://doi.org/10.1016/S0301-9268(96)00050-2

Romer R.L. & Wright J.E. 1992: U–Pb dating of columbites: a geochronological tool to date magmatism and ore deposits. *Geochimica et Cosmochimica Acta* 56, 2137–2142. https://doi.org/10.1016/0016-7037(92)90337-I

Romer R.L., Smeds S.A. & Černý P. 1996: Crystal-chemical and genetic controls of U–Pb systematics of columbite–tantalite. *Mineralogy and Petrology* 57, 243–260. https://doi.org/10.1007/BF01162361

Sarov S., Georgiev N., Naydenov K., Voinova E. & Kolcheva K. 2008: Lithotectonic subdivision of the Western Rhodopes and parts of Eastern Pirin. In: "GEOSCIENCES 2007". *Bulgarian Geological Society,* 89–90.

Schaltegger U., Ulianov A., Müntener O., Ovtcharova M., Peytcheva I., Vonlanthen P., Vennemann T., Antognini M. & Girlanda F. 2015: Megacrystic zircon with planar fractures in miaskite-type nepheline pegmatites formed at high pressures in the lower crust (Ivrea Zone, Southern Alps, Switzerland). *American Mineralogist* 100, 83–94. https://doi.org/10.2138/am-2015-4773

Schmid S., Fügenschuh B., Kounov A., Matenco L., Nievergelt P., Oberhänsli R., Pleuger J., Schefer S., Schuster R., Tomljenović B., Ustaszewski K. & van Hinsbergen D. 2020: Tectonic units of the Alpine collision zone between Eastern Alps and western Turkey. *Gondwana Research* 78, 308–374. https://doi.org/10.1016/j.gr.2019.07.005

Smith S.R., Foster G.L., Romer R.L., Tindle A.G., Kelley S.P., Noble S.R., Horstwood M. & Breaks F.W. 2004: U–Pb columbite–tantalite chronology of rare-element pegmatites using TIMS and Laser Ablation-Multi collector-ICP-MS. *Contributions to Mineralogy and Petrology* 147, 549–564. https://doi.org/10.1007/s00410-003-0538-y

Siachoque A., Garcia R. & Vlach S. 2020: Occurrence and Composition of Columbite-(Fe) In the Reduced A-Type Desemborque Pluton, Graciosa Province (S-SE Brazil). *Minerals* 10, 411. https://doi.org/10.3390/min10050411

Stavrev M., Peytcheva I., Hikov A., Vassileva R., von Quadt A., Guillong M., Grozdev V. & Plotkina Y. 2020: Late Cretaceous magmatism in part of the Western Rhodopes (Bulgaria): U–Pb dating on zircon and grossular-andradite garnets. *Comptes Rendus de l'Acad´emie Bulgare des Sciences* 73, 522–530. https://doi.org/10.7546/CRABS.2020.04.11

Turpaud P. & Reischmann T. 2010: Characterization of igneous terranes by zircon dating: implications for UHP occurrences and suture identification in the Central Rhodope, northern Greece. *International Journal of Earth Sciences* 99, 567–91.

Valkov V., Antova N. & Doncheva K. 1989: Granitoids of the Rila-West Rhodopes Batholith. *Geologica Balcanica* 19, 21–54 (in Russian with English abstract).

Von Quadt A., Guillong M., Laurent O., Peytcheva I. & Galliski M. 2019: U–Pb dating of columbite-bearing ores with a new columbite reference material. *Review of the Bulgarian Geological Society* 80, 94–95.

Yan Q.-H., Qiu Z.-W., Wang H., Wang M., Wei X.-P., Li P., Zhang R.-Q., Li C.-Y. & Liu J. 2018: Age of the Dahongliutan rare metal pegmatite deposit, West Kunlun, Xinjiang (NW China): Constraints from LA–ICP–MS U–Pb dating of columbite-(Fe) and cassiterite. *Ore Geology Reviews* 100, 561–573. https://doi.org/10.1016/j.oregeorev.2016.11.010

Yordanov N., Mareva S. & Halezov I. 1962: Investigations on columbite from Vishteritsa. *Bulletin of the Institutes of General and Inorganic Chemistry and Organic Chemistry* 9, 123–135 (in Bulgarian).

Zhou Q., Qin K., Tang D., Wang C. & Sakyi P. 2018: LA-ICP-MS U–Pb zircon, columbite-tantalite and $^{40}Ar$–$^{39}Ar$ muscovite age constraints for the rare-element pegmatite dykes in the Altai orogenic belt, NW China. *Geological Magazine* 155, 707–728. https://doi.org/10.1017/S0016756816001096